Mon. Not. R. Astron. Soc. **000**, 1–20 (2011) Printed 20 September 2011 (MN LaTeX style file v2.2)

arXiv:1109.3748v1 [astro-ph.EP] 17 Sep 2011

Modelling the Spectra of Planets, Brown Dwarfs and Stars using VSTAR

Jeremy Bailey,[⋆] Lucyna Kedziora-Chudczer

School of Physics, University of New South Wales, NSW 2052, Australia

Accepted 2011 September 16; Received 2011 September 15; in original form 2011 August 23

ABSTRACT

We describe a new software package capable of predicting the spectra of solar-system planets, exoplanets, brown dwarfs and cool stars. The Versatile Software for Transfer of Atmospheric Radiation (VSTAR) code combines a line-by-line approach to molecular and atomic absorption with a full multiple scattering treatment of radiative transfer. VSTAR is a modular system incorporating an ionization and chemical equilibrium model, a comprehensive treatment of spectral line absorption using a database of more than 2.9 billion spectral lines, a scattering package and a radiative transfer module. We test the methods by comparison with other models and benchmark calculations. We present examples of the use of VSTAR to model the spectra of terrestrial and giant planet in our own solar system, brown dwarfs and cool stars.

Key words: radiative transfer – techniques: spectroscopic – planets and satellites: atmospheres – stars: atmospheres – brown dwarfs.

1 INTRODUCTION

Until recently the modelling of the atmospheres of stars (e.g. Gray 2005) and the modelling of the atmospheres of the Earth and other solar-system planets (e.g. Liou 2002) have developed largely independently. Models of stars applied to high temperature objects with effective temperatures $T_{\rm eff} >$ 3000K, with opacity dominated by the line and continuum absorption of atoms and atomic ions, whereas planetary atmosphere models applied to cool objects $T_{\rm eff} \sim$ 100-300K where the important processes were molecular absoprtion and scattering from molecules and cloud particles.

This situation changed with the discovery in the mid-1990s of the first unambiguous brown dwarf, Gl229B. (Nakajima et al. 1995; Oppenheimer et al. 1995) and the first hot Jupiter planets beginning with 51 Peg b (Mayor & Queloz 1995; Marcy et al. 1997). Many more such objects have now been discovered and reveal that planets and brown dwarfs populate an intermediate range of temperatures not explored previously. This has led to the requirement to develop new methods to model these atmospheres that cover the effective temperature range from below 1000K to more than 2000K.

One widely used approach has been to adapt stellar atmosphere codes to handle the lower temperatures encountered in exoplanets and brown dwarfs. Models of this type are described for example by Tsuji et al. (1996), Allard et al. (2001), Barman, Hauschildt & Allard (2001), and Burrows, Sudarsky & Hubeny (2003, 2006). An alternative approach, and the one we follow in this paper, is to take models originally used for the atmospheres of the Earth or other solar system planets and adapt them to handle the higher temperatures needed for exoplanets and brown dwarfs. Such an approach has been described by Marley et al. (2002) and Fortney et al. (2005) who use a model based on one originally used to model the atmospheres of Titan and Uranus (McKay et al. 1989; Marley & McKay 1999).

One important difference between the techniques used in stellar atmosphere modelling and in Earth atmosphere modelling is the approach to radiative transfer. In stellar atmospheres simplified treatments of scattering, such as the assumption of isotropic scattering, are commonly adopted. This is justified by the fact that scattering is in most cases not an important source of opacity in stellar atmospheres, and where it does become significant, in the form of Rayleigh scattering from molecules in cool stars, and scattering from electrons in hot stars, the phase functions are forward-backward symmetric. Scattering from clouds and aerosols in the Earth atmosphere can, however, result in strongly forward peaked phase functions, and to properly model such cases radiative transfer methods that more rigorously handle multiple scattering with anisotropic phase functions are needed. While these techniques build on the classic work of

---

[⋆] E-mail: j.bailey@unsw.edu.au

astronomers such as Chandrasekhar and van de Hulst, much recent development of such methods has been in the context of Earth atmosphere research (e.g. Liou 2002).

Clouds are now known to be important not just in the atmospheres of all the solar system planets, but in many brown dwarfs and even in late M dwarfs. Thus for all these objects a more rigorous treatment of radiative transfer is desirable. Such an approach is particularly important for modelling the reflected light from exoplanets, because the angular dependence of scattering is an important factor in determining the phase variation around a planet's orbit (e.g. Seager, Whitney & Sasselov 2000; Cahoy, Marley & Fortney 2010).

In this paper we describe the methods used in the VSTAR (Versatile Sofwtware for Transfer of Atmospheric Radiaition) atmospheric modelling software. VSTAR was originally developed as a way of modelling the spectra of the solar system planets, and an early version of it is described by Bailey (2006). In this paper we describe the current version of VSTAR which can now handle a wide range of atmospheres ranging from those of the coolest solar system planets up to stars with temperatures of ∼3000K, and thus including the brown dwarfs and hot Jupiter type exoplanets.

2 THE VSTAR MODEL

2.1 Ionization and Chemical Equilibrium

The Ionization and Chemical Equilibrium (ICE) package of VSTAR is used to determine the equilibrium chemical composition of an atmospheric layer given its elemental abundances, pressure and temperature. ICE handles gas phase chemistry, ionized species and the formation of solid and liquid condensates. Full details of the methods employed in this package will be described elsewhere so only a brief description is given here. The techniques used are similar to those described by Tsuji (1973), Allard et al. (2001) and Lodders & Fegley (2002). For each compound considered in the model the equilibrium constant of formation K_f from the elements is required. These are used in a set of equations for the mass balance of each element, and for the charge balance to solve for the abundances of each molecular species. K_f is related to the Gibbs free energy of formation $\Delta_f G^o$ through:

$$\Delta_f G^o = -RT \ln K_f \qquad (1)$$

Where R is the gas constant. This relationship is indicative of the link between the technique we use based on equilibrium coinstants, and the alternative technique for chemical models based on minimization of the total Gibbs free energy of the system (Sharp & Huebner 1990; Sharp & Burrows 2007) Both $\Delta_f G^o$ and K_f are functions of temperature (T) and are available in standdard compilations of thermochemical data. Our main source of thermochemical data was the fourth edition of the NIST-JANAF thermochemical tables (Chase 1998). We used data from Lodders (1999) and Lodders (2004) for several compounds for which the JANAF data have been shown to contain errors. Additional sources of thermochemical data were Barin (1995) and Robie & Hemingway (1995).

Some important species, however, do not have data in any of these tabulations, and for some others the available data do not extend to sufficiently high temperatures for stellar atmosphere models. For a number of gas-phase species we have therefore calculated our own thermochemical data. To do this we first calculate the partition function using the spectroscopic constants of the molecule. We use a rigid rotator harmonic oscillator model (with additonal corrections for anharmonicity and centrifugal distortion) for the rotational and vibrational levels, and direct summation over the electronic levels (Mayer & Mayer 1940). The thermodynamic functions can then be derived from the partition function and the dissociation energy of the molecule. The techniques are essentially the same as those used in constructing the NIST-JANAF thermochemical tables (Chase 1998) for gas phase species, and we have tested our methods by reproducing results published in these tables. Species we have calculated new thermochemical data for include FeH, CrH, CaH, TiH, RbCl and RbF.

Our thermochemical model currently includes 143 gas-phase and condensed-phase compounds of 27 elements. While this is not as extensive as some other models, we have been careful to include all species listed as important in previous studies such as Burrows & Sharp (1999). Our chemical model predictions show good agreement with previous results such as those of Lodders & Fegley (2002) and Sharp & Burrows (2007). Figure 1 shows the results of calculations of the mixing ratios, or mole fractions, for a number of important species at 1 atmosphere pressure over a range of temperatures. It can be directly compared with figure 17 of Sharp & Burrows (2007). The model can easily be expanded by adding new species to our thermochemical database.

Our current model assumes true equilibrium chemistry in that when condensates form, the condensed phase is assumed to remain in equilibrium with the gas phase. This assumption is commonly made in such models. However, it may not be true in real cases since condensed material can fall under gravity and rain out of the system. Models that take account of this "rainout" process are described by Marley et al. (2002) and Freedman et al. (2008).

2.2 Molecular Absorption Lines

Absorption lines due to rovibrational and electronic transitions of molecules are the most important features of the spectra of planets, brown dwarfs and the coolest stars. For use with VSTAR we have collected a line database that currently contains more than 2.9 billion lines. The line lists used with VSTAR are listed in table 1. The line parameters are in a variety of different formats. The essential data needed for all lines are the line position (as wavelength or wavenumber), the line intensity, and the lower state energy of the transition (ususally given in cm^{-1} or eV).

Line intensity is usually given in one of three forms. HITRAN, GEISA (see section 2.2.1) and similar lists give a line intensity S_0 in units of cm $\mathrm{molecule}^{-1}$ (sometimes given as $\mathrm{cm}^2\ \mathrm{mol}^{-1}\ \mathrm{cm}^{-1}$) at a reference temperature T_0. For HITRAN T_0 is 296 K, but some other lists use a different reference temperature.

The line intensity at temperature T is then calculated using (Rothman et al. 1998):

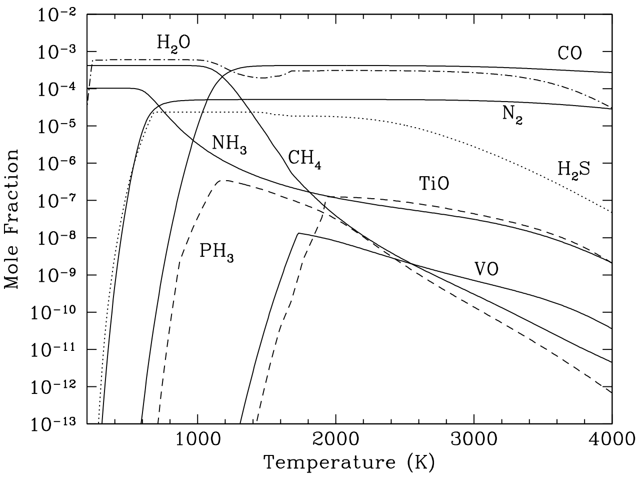

Figure 1. Mixing ratios on several important species as a function of temperature for a solar composition gas at 1 atm pressure calculated with our chemical equilibrium model. The results can be compared with figure 17 of Sharp & Burrows (2007)

$$S = \frac{S_0 Q(T_0)}{Q(T)} \frac{\exp(-c_2 E_l/T)}{\exp(-c_2 E_l/T_0)} \frac{[1-\exp(-c_2\nu_0/T)]}{[1-\exp(-c_2\nu_0/T_0)]} \qquad (2)$$

where ν_0 is the line frequency in cm^{-1}, E_l is the lower state energy in cm^{-1}, c_2 is the second radiation constant ($= hc/k$) and $Q(T)$ is the partition function (or total internal partition sum).

Line intensities may also be quoted in the form of Einstein A coefficients (A_{21}). The line intensity S (in cm/mol) at a temperature T can be calculated from A_{21} using (Šimečková et al. 2006).

$$S = \frac{gA_{21}}{8\pi c\nu_0^2 Q(T)} \exp(-c_2 E_l/T)(1-\exp(-c_2\nu_0/T)) \qquad (3)$$

Here g is the statistical weight of the upper level of the transition. In most cases g can be written as $(2J+1)g_s$ where J is the rotational quantum number of the upper state, and g_s is the nuclear spin degeneracy. Different formulae are needed if hyperfine structure is included in the line list (see Šimečková et al. 2006). The g_s used in equation 3 needs to be consistent with that used in calculating the partition function (see section 2.5.2).

In astronomical line lists, such as those of Kurucz (2005), the oscillator strength f, usually tabulated as gf or $\log(gf)$ (where g is the statistical weight) is the usual form for listing line strengths. The line intensity at temperature T can be calculated from gf using:

$$S = \frac{\pi g f e^2}{m_e c^2 Q(T)} \exp(-c_2 E_l/T)(1-\exp(-c_2\nu_0/T)) \qquad (4)$$

where e is the electron charge, m_e is the electron mass and other symbols are as above.

2.2.1 HITRAN and GEISA

HITRAN (HIgh resolution TRANsmission) and GEISA (Gestion et Etude des Informations Spectroscopiques Atmosphériques) are compilations of molecular spectroscopic parameters designed primarily for the Earth atmosphere, but often useful for the atmospheres of other planets. Both are updated every few years with the most recent releases being HITRAN 2008 (Rothman et al. 2009) and GEISA 2009 (Jacquinet-Husson et al. 2008). The line parameters are generally best suited to low temperature models and more complete line lists are usually needed for higher temperature atmospheres such as those encountered in brown dwarfs, hot Jupiter type planets and stars. For example Bailey (2009) showed that HITRAN and GEISA were significantly incomplete for water vapour line parameters at temperatures of 500-700K encountered in the Venus lower atmosphere.

2.2.2 HITEMP

The HITEMP database is a companion to HITRAN containing line data suitable for use at higher temperatures. The latest edition of HITEMP was released in 2010 (Rothman et al. 2010) and replaces an earlier edition described by Rothman et al. (1995). HITEMP contains data for five species, H_2O, CO_2, CO, NO and OH. The data format is the same as that used in HITRAN, and HITEMP is consistent with HITRAN, in the sense that lines common to both databases have the same line parameter values, although HITEMP includes many lines not in HITRAN.

2.2.3 Water Vapour — H_2O

Water vapour is an important absorber in atmospheres ranging from stars to the terrestrial planets. A number of line lists are available for water vapour at high temperatures. These include the HITEMP list (Rothman et al. 2010), the SCAN list (Jørgensen et al. 2001), the list of Partridge & Schwenke (1997) and the BT2 list (Barber et al. 2006). Comparisons of the various lists have been reported by Allard et al. (2000), Jones et al. (2003) and Bailey (2009). We normally use the BT2 list which is the most extensive and is based on the acurate dipole moment surface of Schwenke & Partridge (2000). The HITEMP list for H_2O is based on BT2.

BT2 includes only the main isotopologue of water ($H_2{}^{16}O$). The VTT list of Voronin et al. (2010) provides a similar list for HDO. In the atmosphere of Venus deuterium is enhanced over terrestrial abundances by a factor of 100–150 so HDO absorption is significant. Line data for a range of other isotopologues of water at 296K and 1000K are available from the Spectra Information System (http://spectra.iao.ru) at the Institute of Atmospheric Optics, Tomsk. These data are based on the analysis of Schwenke & Partridge (2000).

2.2.4 Carbon Dioxide — CO_2

Carbon dioxide is an important constituent of terrestrial planet atmospheres. Until recently it has not been thought to be important in giant planet atmospheres. However, recent results from transitting extrasolar planets (Swain et al.

Table 1. Molecular Line Lists used with VSTAR

Molecule	List	Number of Lines	Reference
39 molecules	HITRAN 2008	2,713,968	Rothman et al. (2009)
50 molecules	GEISA 2009	3,807,997	Jacquinet-Husson et al. (2008)
H_2O	BT2	505,806,202	Barber et al. (2006)
H_2O	SCAN	101,455,143	Jørgensen et al. (2001)
H_2O		65,912,356	Partridge & Schwenke (1997)
H_2O	HITEMP	111,377,777	Rothman et al. (2010)
HDO	VTT	697,454,528	Voronin et al. (2010)
CO_2		7,088,178	Pollack et al. (1993)
CO_2	HITEMP	11,377,777	Rothman et al. (2010)
CO_2	CDSD-296	419,610	Tashkun et al. (2003)
CO_2	CDSD-1000	3,950,553	Tashkun et al. (2003)
CO_2	CDSD-Venus	11,730,277	Tashkun et al. (2003)
CO	HITEMP	115,218	Rothman et al. (2010)
CO		134,421	Goorvitch (1994)
CH_4 (cool)		339,690	see text (section 2.2.6)
CH_4 (hot)		134,862,336	see text (section 2.2.6)
NH_3		3,249,988	Yurchenko et al. (2009)
NH_3	BYTe	1,138,323,351	Yurchenko, Barber & Tennyson (2011)
TiO	SCAN	12,837,150	Jørgensen (1994)
TiO		37,744,499	Schwenke (1998)
TiO		11,369,552	Plez (1998)
VO		3,171,552	Plez, B., private communication
CaH		124,615	see text (section 2.2.9)
MgH		23,315	Weck et al. (2003); Skory et al. (2003)
MgH		119,167	Kurucz (2005)
FeH (F-X)		116,300	Dulick et al. (2003)
FeH (E-A)		6,357	Hargreaves et al. (2010)
CrH		14,255	Burrows et al. (2002)
TiH		199,073	Burrows et al. (2005)
CH	SCAN	114,567	Jørgensen et al. (1996)
CN	SCAN	2,245,378	Jørgensen & Larsson (1990)
C_2		360,887	Querci, Querci & Kunde (1971); Querci, Querci & Tsuji (1974)
HCN/HNC		34,433,190	Harris et al. (2006)

2009a,b) suggest CO_2 may be important in these atmospheres as well. Recently CO_2 has also been detected in brown dwarfs (Yamamura, Tsuji & Tanabe 2010). At low temperatures HITRAN, GEISA or CDSD-296 (Carbon Dioxide Spectroscopic Databank, Tashkun et al. 2003) can be used. High temperature line lists include the list described by Pollack et al. (1993) and the CDSD-1000 list (Tashkun et al. 2003). The latter list contains more than 3 million lines and is complete to an intensity of 10^{-27} cm mol^{-1} at 1000 K.

The dense CO_2 atmosphere of Venus provides a particular challenge to the modelling of CO_2 absorption with pressures up to 90 bars of almost pure CO_2 and requires a line list with a much deeper intensity cutoff than is normally necessary. The list of Pollack et al. (1993) is the one that has normally been used for modelling the Venus deep atmosphere. However, an alternative is the CDSD-Venus list, a version of the CDSD list with a deeper cutoff of 10^{-30} cm mol^{-1} at 750 K.

The HITEMP (Rothman et al. 2010) list for CO_2 is based on the CDSD line lists.

2.2.5 Carbon Monoxide — CO

Carbon monoxide is significant in terrestrial planet atmospheres, and is also observed in Titan. It also becomes important in high temperature atmospheres where equilibrium chemistry favours CO over CH_4. For high temperatures the HITEMP line list (Rothman et al. 2010) or the list of Goorvitch (1994) can be used.

2.2.6 Methane — CH_4

Methane is an important absorber in the atmospheres of the solar system giant planets and in Titan. It has been detected in the atmospheres of extrasolar giant panets (Swain et al. 2008). It is also important in brown dwarfs, the presence of methane absorption features in the near-IR being the defining characteristic of the T-dwarf class.

However, methane has a complex spectrum due to the presence of coincidences between its four vibrational modes that result in a series of interacting states known as polyads, spaced at intervals of about 1500 cm^{-1}. Most line data is either based on experimental measurements or on effective Hamiltonian models, which exist only for the lowest few polyads. The Spherical Top Data System (STDS) software of Wenger & Champion (1998) can be used to generate line lists from these effective Hamiltonian models. A good model has recently been obtained (Albert et al. 2009) for the ground-state and the lowest three polyads (the Dyad, Pentad and Octad) and this allows reliable prediction of the low temperature methane spectrum from 0 – 4800 cm^{-1}.

This model is used in the 2008 update of the methane line parameters in HITRAN (Rothman et al. 2009). A preliminary model is available for the next polyad, the Tetradecad (Boudon, Rey & Loete 2006; Robert et al. 2001).

Above 4800 cm^{-1} many of the line parameters included in HITRAN are empirical measurements at room temperature originating from Brown (2005). These mostly lack lower state energies (HITRAN lists fictitious lower state energies of 555.5555 or 333.3333) and so cannot be used to derive reliable line intensities at other temperatures. However, some lines in the 5500 – 6150 cm^{-1} region have empirical lower state energies derived from measurements at multiple temperatures from Margolis (1990) and Gao et al. (2009).

Recently much improved data for the low temperature methane spectrum over the range 1.26 – 1.71 μm (5852 — 7919 cm^{-1} has become available from laboratory measurements described by Wang, Kassi & Campargue (2010); Wang et al. (2011), Campargue et al. (2010) and Mondelain et al. (2011). These data are based on a combination of room temperature and cryogenic (∼80K) measurements that allow empirical determinations of lower state energies, and includes deep cavity ring down spectroscopy of the weak lines in the window regions between the strong absorption band systems. An application of this list to the spectrum of Titan is reported by de Bergh et al.. (2011).

For low temperature atmospheres, such as the solar system giant planets or Titan, we use a composite list that combines the laboratory data described above, as well as data described by Nikitin et al. (2010, 2011), with HITRAN data from 0 – 4800 cm^{-1}. We use STDS to fill in the remaining gap in coverage between 4800 and 5500 cm^{-1}. An early version of this list and its application to Titan is described by Bailey et al. (2011). The current version of the list is further improved by including the most recent data of Wang et al. (2011) and Mondelain et al. (2011).

For high temperature atmospheres, such as those of brown dwarfs and hot Jupiters, we use a line list computed with the STDS software (Wenger & Champion 1998) up to J=60 for most band systems, and up to J=50 for the most complex system modelled (the Tetradecad-Pentad). This gives a list of nearly 135 million lines. Because the effective Hamiltonian model of Albert et al. (2009) involves high order polynomial fits to empirical data usually limited to the range up to J=20-30, it is not suitable for extrapolation to these high J values. We instead use the low order effective Hamiltonian parameters of Borysov et al. (2002). These provide a poorer fit to observed line positions (~ 0.5 cm^{-1}) but allow more reliable extrapolation to high J. For most purposes we use a smaller list extracted from the full list with a line intensity cutoff of 10^{-27} cm mol^{-1} at 1500 K giving a list of 15.8 million lines.

While this approach to the hot methane spectrum is similar to that used by other groups modelling brown dwarf and exoplanet spectra (e.g. Freedman et al. 2008; Homeier et al. 2003; Borysov et al. 2002) it is important to understand that while these models include high rotational levels, they do not include higher vibrational levels that are needed at these temperatures and many hot band systems are therefore missing. Methane band strengths will therefore be underestimated by amounts that will increase for shorter wavelengths and higher temperatures.

Above 6500 cm^{-1} there is little useful methane line data for high temperatures. The low temperature line list can be used but will omit both hot bands and high J transitions. An alternative is available in the form of low resolution absorption coefficients, band models or k-distribution parameters for methane (Strong et al. 1993; Irwin et al. 2006; Karkoschka & Tomasko 2010). The first two sets cover the near-IR, and the latter extends through the visble as well. However, these data are not in an ideal form for use with line-by-line programs such as VSTAR and are not designed for high temperature use. The optimal way to use such datasets is in conjunction with the correlated-k method (Goody et al. 1989).

2.2.7 Ammonia — NH_3

Ammonia is present in the atmospheres of Jupiter and Saturn, and is also found in cool brown dwarfs where it is seen most easily through a feature at 10.5 μm (Cushing et al. 2006). The spectrum of ammonia, has until recently, presented similar problems to methane. The line parameters in HITRAN only include lines up to 5295 cm^{-1} and have not been updated since the 2000 edition. However, recently a new line list (the BYTe list) for hot NH_3 (up to ∼1500 K) has been published by Yurchenko et al. (2011). It contains more than 1.1 billion lines covering the range 0 – 12,000 cm^{-1}. An NH_3 list for use up to 300K and covering 0 – 8000 cm^{-1} was described by Yurchenko et al. (2009).

2.2.8 Metal Oxides — TiO and VO

Bands of Titanium Oxide (TiO) and Vanadium Oxide (VO) are distinctive features of the spectrum of M-type stars. There are several line list available for TiO from Jørgensen (1994), Schwenke (1998) and Plez (1998). The lists cover five isotopologues of the TiO molecule. Comparisons of the lists can be found in Allard et al. (2000) and Pavlenko et al. (2006). The VSTAR database also includes a VO line list provided by Plez, B. (private communication), which is part of the line lists assembled by Gustafsson et al. (2008).

2.2.9 Metal Hydrides — CaH, MgH, FeH, CrH and TiH

Bands due to electronic transitions of metal hydrides are seen in M-type stars and some cooler objects. A line list for MgH is described by Weck et al. (2003) and Skory et al. (2003). This list, and a similarly formatted list for CaH (which does not appear to have a published description) can be found on the web site of the University of Georgia Molecular Opacity Project[1]. An alternative MgH list which includes two additional MgH isotopologues is available from Kurucz (2005).

Lines lists are also available for FeH (Dulick et al. 2003), CrH (Burrows et al. 2002) and TiH (Burrows et al. 2005). These line lists are all similarly formatted. They cover only the most abundant isotopologue of each molcule, though methods for determining line positions for other isotopologues are described. The Dulick et al. (2003) line list for FeH covers the F-X band, but absorptions in the E-A band

[1] http://www.physast.uga.edu/ugamop/index.html

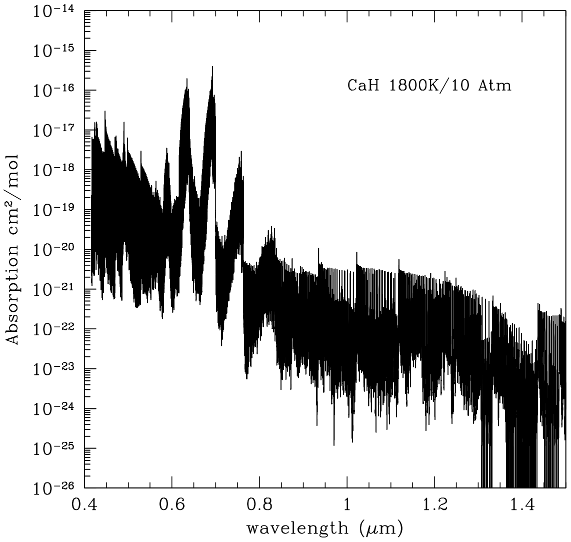

Figure 2. Monochromatic absorption (in cm^2 $molecule^{-1}$) of CaH at a temperature of 1800 K and a pressure of 10 atm

are also important in the 1.6 μm region. These are available from a recent empirically based line list described by Hargreaves et al. (2010).

2.2.10 CH, CN and C_2, HCN/HNC

These bands are present in cool stars and become particularly strong in carbon stars. Line lists available from Jørgensen et al. (1996) (CH), Jørgensen & Larsson (1990) (CN), Querci et al. (1971) and Querci et al. (1974) (C_2) and Harris et al. (2006) (HCN/HNC) are included in the VSTAR database.

2.2.11 Absorption Plots

Sharp & Burrows (2007) have presented plots of the monochromatic absorption (in cm^2 $molecule^{-1}$) for many molecular species present in brown dwarf or giant exoplanet atmospheres. We have made similar plots for the molecular species described above. In all but one case our plots look essentially the same as those given by Sharp & Burrows (2007). The exception is CaH where our absorption plot, given in figure 2, shows the well known absorption bands at 0.638 and 0.683 μm in M dwarfs, which are absent in figure 9 of Sharp & Burrows (2007) for the same temperature and pressure.

2.3 Atomic Lines

While molecular lines are most important in the coolest objects, lines of the alkali metals are significant in brown dwarfs and exoplanets, and many other atomic lines become important in M stars. VSTAR can make use of atomic line data in the format of the Kurucz line lists, or that of the Vienna Atomic Line Database (VALD, Piskunov et al. 1995; Kupka et al. 1999).

2.4 Line Profiles

The default treatment of spectral line profiles in VSTAR is to use a Voigt line shape in the line core, approximated using the methods described by Humlicek (1982) and Schreier (1992), out to 20 Doppler widths from the line centre. In the line wings a van-Vleck Weisskopf profile is used which has a line shape function $\phi(\nu)$ of the form (van Vleck & Weisskopf 1945):

$$\phi(\nu) = \frac{1}{\pi}\left(\frac{\nu}{\nu_0}\right)\left[\frac{\gamma}{(\nu-\nu_0)^2+\gamma^2} + \frac{\gamma}{(\nu+\nu_0)^2+\gamma^2}\right] \quad (5)$$

Where ν is frequency, ν_0 is the line centre frequency, and γ is the line half width. In most cases this is essentially identical to a Lorentzian, but this profile provides the asymmetry that is needed at microwave wavelengths or with very broad lines, and goes to zero at zero frequency.

In general it is found that continuing this profile out to large distances from the line centre overestimates the absorption in the far wings. In cases where the precise far wing behaviour is important, VSTAR allows the line wings to be modified by multiplying by a correction factor, usually called a χ factor. For example the far line wings of CO_2 are known to be sub-Lorentzian (Perrin & Hartmann 1989; Tonkov et al. 1996), and the correct profile is important in modelling the spectra of the "windows" in the Venus nightside spectrum (e.g. Meadows & Crisp 1996).

Where the precise line wing shape is not critical, it is usually sufficient to cut off the line profiles at a distance from the line centre, which can be chosen according to the typical line strengths and widths but usually ranges from 20 to 100 cm^{-1}. This approach improves the speed of computation. In either this case, or the χ factor case, the line intensities are adjusted to ensure that the integrated line strength is not changed from its original value.

The line profile requires a value for the pressure broadened line half width (γ in equation 5). HITRAN, GEISA and similarly formatted files such as HITEMP and CDSD include line width data in the form of an air broadened line half width coefficient γ_0 (in cm^{-1} atm^{-1}, quoted for the reference temperature T_0), a self broadened line half width, and a temperature exponent n for the line width such that:

$$\gamma(T) = \gamma_0 \left(\frac{T_0}{T}\right)^n \quad (6)$$

Line widths for different transitions of a molecule vary, and are usually found to depend primarily on the rotational quantum numbers of the levels involved in the transition. Variation with the vibrational quantum numbers is much smaller, and is often ignored in empirical models for the line shape.

Line widths depend on the type of gas responsible for the broadening. Hence the air broadened widths given in HITRAN type files are not usually what is needed, as we generally want the line widths for broadening in H_2 and He (for giant planet and brown dwarf atmospheres) or CO_2

Table 2. Relative broadening effects of different broadening gases

Lines	Broadened by							References
of	H_2	He	N_2	O_2	CO_2	Air	H_2/He	
NH_3	0.832	0.370	1.0	0.693		0.939	0.818	Brown & Peterson (1994)
CH_4	1.017	0.643	1.0	0.943		0.989	0.961	Pine & Gabard (2003)
CO	0.85	0.64	1.0	0.90	1.30	0.98	0.82	Burch et al. (1962), Hartmann et al. (1988)
H_2O	0.777	0.221	1.0	0.661	1.50	0.932	0.694	Gamache et al. (1996)
CO_2	1.41	0.59	1.0	0.81	1.20	0.962	1.287	Burch et al. (1969)

(for terrestrial planets). Unfortunately the data available on these alternate broadening gases is rather incomplete.

Table 2 shows the relative line widths due to broadening in different broadening gases, averaged over many transitions. The line widths are relative to that due to broadening in N_2. Some general trends can be identified in the table. For example, helium always produces the smallest broadening. O_2 broadening is always less than that due to N_2. CO_2 produces the largest broadening, However, H_2 is sometimes less than, and sometimes more than N_2. These trends can be used as a rough guide, when no broadening information is available for a specific broadening gas.

Broadening for a mixture of gases can be obtained by averaging the broadening coefficients weighted by their partial pressures (or volume mixing ratios). Table 2 gives values for air (taken as 80% N_2, 20% O_2) and an H_2/He mixture typical of a giant planet or brown dwarf atmosphere (85% H_2, 15% He) obtained from the other values in the table.

VSTAR includes specific models for the line widths of several of the more important gases. For H_2O broadened in CO_2 we use the model described by Bailey (2009) based on the data of Delaye et al. (1989). For H_2O broadened in H_2 and He we use the data from Gamache et al. (1996). For NH_3 broadened by H_2, He, N_2 and O_2 we use the results of Brown & Peterson (1994) for the dependence of width on the J and K quantum numbers, and the temperature exponents are from Nouri et al. (2004). For CO we use the model for the J dependence from HITRAN (Rothman et al. 2005) for air, and from Régalia-Jarlot et al. (2005) for H_2. When CH_4 line data are taken from HITRAN, the air broadened width from HITRAN is used for H_2/He broadening also, since table 2 shows little difference in the two cases. For other sources of CH_4 line data the broadening is based on data from Pine (1992).

Atomic line lists usually give width data in the form of three coefficients for natural (γ_n), van der Waals (γ_w) and Stark (γ_s) broadening. Stark broadening is usually negligible at the temperatures considered here. The line width γ needed for equation 5 can be calculated from:

$$\gamma = \frac{1}{4\pi c}\left[\gamma_w(N_H + c_1 N_{H_2} + c_2 N_{\mathrm{He}})\left(\frac{T}{10,000}\right)^{0.3} + \gamma_n\right] \tag{7}$$

where N_H, N_{H_2} and N_{He} are the number densities of atomic hydrogen, molecular hydrogen and helium. c_1 and c_2 are coefficients for the relative broadening effects of H_2 and He as compared with H, which can be derived from the polarizabilities of the different species. If γ_w and γ_n are not available they are calculated using methods described by Kurucz & Avrett (1981).

2.5 Partition Functions

The calculation of line intensities from data tabulated in the line lists using equations 2, 3 or 4 requires the partition function $Q(T)$ of the molecule or atom defined by.

$$Q(T) = \sum g_i \exp\left(\frac{-E_i}{kT}\right) \tag{8}$$

where E_i is the energy of level i relative to the ground state, g_i is its statistical weight, and the sum is to be taken over all rotational, vibrational and electronic levels.

2.5.1 Molecular Partition Functions

VSTAR uses molecular partition functions from a range of sources. Polynomial approximations for the partition functions of many molecules for temperatures from 1000 K up to 9000 K or higher are given by Sauval & Tatum (1984) and Irwin (1981). A subroutine for calculating the partition functions of all molecules and isotopologues in HITRAN is provided with that database and is described by Fischer et al. (2003). The HITRAN partition functions are valid over the temperature range from 70 to 3000 K. An updated version of the HITRAN partition functions has recently been published by Laraia et al. (2011), but the work described in this paper used the earlier versions from Fischer et al. (2003). Partition functions can be reconstructed from data in the NIST-JANAF thermochemical tables (Chase 1998). These tables do not list the partition functions explicitly, but the thermochemical properties listed for gas phase substances are derived from partition functions. The partition function can be calculated from the tabulated data using methods described by Irwin (1988).

Partition functions can also be calculated directly from spectroscopic constants using methods already described in section 2.1. In some cases it is possible to calculate molecular partition functions by direct summation over energy levels as in the partition functions for H_2O from Vidler & Tennyson (2000) and CH_4 from Wenger et al. (2008).

2.5.2 Partition Functions and Nuclear Spin

In comparing the molecular partition functions from different sources it was noticed that the partition functions from HITRAN (Fischer et al. 2003) had values which were larger than those from most other sources by integer factors. This is due to the use in HITRAN of a different convention for the treatment of nuclear spin states. The convention in astrophysics is not to count nuclear spin states as distinct states in equation 8. As stated by Irwin (1981), "the statistical weights are divided by ... the product of the nuclear spin statistical weights". It is clear from the descriptions of the HITRAN partition functions in Fischer et al. (2003), Šimečková et al. (2006) and Laraia et al. (2011) that a different convention is adopted in HITRAN, and some other spectroscopy literature, where the corresponding statistical weights include nuclear spin states.

The consequence is that on the HITRAN convention, partition functions Q_{HIT} are numerically larger than astrophysical partition functions Q_{ast} by a factor defined as follows:

$$Q_{\mathrm{HIT}}(T) = Q_{\mathrm{ast}}(T) \prod_{j=1}^{n} (2I_j + 1) \tag{9}$$

where I_j are the nuclear spins of the n atoms contained in a molecule. With $I = 0$ for carbon and oxygen, $^1/_2$ for hydrogen and 1 for nitrogen, these factors becone 4 for H_2O, 16 for CH_4 and 24 for NH_3.

In many cases (e.g. equation 2) partition functions are divided such that these integer factors will cancel out. However, this is not the case when line intensities are calculated from Einsten A coefficients using equation 3. In this case it is important that the statistical weights (g_s) and partition function use the same convention. For example for H_2O lines, if an astrophysical partition function is used the statistical weights for the ortho and para states of water are $^3/_4$ and $^1/_4$, but if the HITRAN partition function is used they are 3 and 1.

2.5.3 Atomic Partition Functions

Partition functions for atoms and atomic ions in VSTAR are calculated using a modified version of the PFSAHA subroutine taken from the ATLAS9 software of Kurucz[2].

2.6 Continuum Processses

A number of continuum absorption processes are included in VSTAR as described in table 3.

2.6.1 Bound-Free and Free-Free Continuum Absorption

Bound-free and free-free absorptions of a number of species are important in stellar atmospheres, and some of these processes remain significant at the cooler temperatures of hot Jupiters and brown dwarfs. The processes included in VSTAR are listed in table 3. These processes are sufficient for the range of temperatures and wavelengths currently studied using VSTAR. A wider range of continumm processes would need to be incorporated to extend the applicability of VSTAR to higher temperatures and into UV wavelengths (see e.g. Sharp & Burrows 2007; Gustafsson et al. 2008).

Table 3. Continuum absorption processes in VSTAR

Process	Reference
H^- free-free	Bell & Berrington (1987)
H^- bound-free	Wishart (1979)
H bound-free and free-free	Gray (2005) pp149-154
H_2^- free-free	Bell (1980)
H_2 - H_2 CIA	Borysow (2002)
	Borysow et al. (2001)
H_2 - He CIA	Borysow et al. (1997, 1989)
	Borysow & Frommhold (1989)
O_2 - O_2 and O_2 - N_2 CIA	Smith & Newnham (1999, 2000)
H_2 - N_2 CIA	McKellar (1989)

2.6.2 Collision Induced Absorptions

Collision induced absorption (CIA) due to H_2 - H_2 pairs is important in the solar system giant planets where it shows up a distinct strong spectral feature at 2.1 μm (see figure 5 for the spectrum of Jupiter in this region). This absorption is also important in brown dwarf, hot jupiters, and M dwarfs. We incorporate this absorption by interpolating in tables provide by Borysow[3]. Three different tables are needed to cover the full temperature range using calculations by Borysow (2002) (60 – 350 K and 400 – 1000 K) and Borysow et al. (2001) (1000 – 7000 K). H_2 - He collision induced absorption is also included using data from Borysow et al. (1997), Borysow et al. (1989) and Borysow & Frommhold (1989).

Other collision induced absorptions included in VSTAR are absorption in the O_2 near infrared bands (Smith & Newnham 1999, 2000) which is needed for the Earth atmosphere, and H_2 - N_2 collision induced absorption which occurs in the Titan atmosphere and for which data is available from McKellar (1989).

.

2.7 Scattering

Scattering processes are often treated in stellar atmosphere codes as just an additional source of opacity which can be added to that due to gas absorption. However, VSTAR uses a more rigorous treatment that requires a full description of scattering. In addition to the optical depth contribution, we need to know the single scattering albedo, ϖ and the phase function, $P(\theta)$, that describes the angular distribution of scattered light.

Single scattering albedo is defined as:

$$\varpi = \frac{\sigma_s}{\sigma_s + \sigma_a} = \frac{\sigma_s}{\sigma_e} \tag{10}$$

where σ_e, σ_a and σ_s are the extinction, absorption and scattering cross sections per particle.

2.7.1 Rayleigh Scattering from Molecules

VSTAR includes models for the Rayleigh scattering due to air, H, H_2, He, N_2 and CO_2 or any mixture of these gases. The wavelength dependence of the scattering cross section of H_2 is from Dalgarno & Williams (1962). Those of H and He are from Dalgarno as cited by Kurucz (1970).

---

[2] http://kurucz.harvard.edu/programs/atlas9

[3] http://www.astro.ku.dk/ aborysow/programs

For the other gases the scattering cross section (σ) is derived from the refractive index of the gas using (Hansen & Travis 1974):

$$\sigma = \frac{8\pi^3(n(\lambda)^2 - 1)^2}{3\lambda^4 N^2} F_K \tag{11}$$

where $n(\lambda)$ is the wavelength dependent refractive index, λ is wavelength and N is the number density (molecules cm^{-3}) of the gas measured at the same temperature and pressure as the refractive index. F_K is known as the King factor and is given by:

$$F_K = \frac{6 + 3\delta}{6 - 7\delta} \tag{12}$$

where δ is the depolarization factor. For air we use the refractive index wavelength dependence from Peck & Reeder (1972) and the King factor from Young (1981). For CO_2 the refractive index is from Old et al. (1971) and the King factor is from Sneep & Ubachs (2005). For N_2 the refractive index is from Cox (2000).

Rayleigh scattering is pure scattering so it has a single scattering albedo of one, and the phase function is:

$$P(\theta) = \frac{3}{4}(1 + \cos^2\theta) \tag{13}$$

2.7.2 Scattering from Particles

Scattering from liquid or solid particles suspended in the atmosphere (variously called clouds, aerosols or condensates) occurs in all planetary atmospheres in the solar system, and in brown dwarfs and M stars.

Particle scattering can be modelled using Lorenz-Mie theory, which provides a solution to Maxwell's equations that describes scattering of light from a homogenous sphere with a complex refractive index $n + ik$, and a size parameter $x = 2\pi r/\lambda$ where r is the radius of the sphere, and λ is the wavelength. VSTAR uses a Lorenz-Mie scattering code from Mishchenko et al. (2002) that models scattering from a size distribution of spherical particles. The particle size distribution can be described by a number of functional forms including power law, log normal and gamma distrbutions. VSTAR can handle up to 20 particle modes, each with its own wavelength dependent refractive index, particle size distribution, and vertical distribution in the atmosphere.

The scattering code generates the extinction and scattering cross sections per particle (σ_e and σ_s) which give the single scattering albedo according to equation 10.

It also provides the phase function $P(\theta)$ both as an array of values for different scattering angles, and as an expansion in Legendre polynomials

$$P(\theta) = \sum_{s=0}^{s_{\max}} \alpha^s P_s(\cos\theta) \tag{14}$$

which is the form required for the discrete-ordinate radiative transfer code described in section 2.8.

If the particles are genuinally spherical (e.g. liquid droplets) then the phase function derived from the Lorenz-Mie code is appropriate. Sometimes however, spherical models are used simply as a generic representation of solid particles which probably have a range of irregular shapes In this case the full spherical particle phase function is probably not a good representation. It will include angular structure in the form of features such as rainbows and glories, that are specific to the particles' sphericity, and disappear for non-spherical particles (Bailey 2007). In this case a better representation may be the Henyey-Greenstein phase function (Henyey & Greenstein 1941):

$$P_{\mathrm{HG}}(\theta) = \frac{1 - g^2}{4\pi(1 + g^2 - 2g\cos\theta)^{3/2}} \tag{15}$$

where g is the asymmetry parameter defined by:

$$g \equiv \langle\cos\theta\rangle = \int_0^{\pi} \cos\theta P(\theta) 2\pi \sin\theta \, d\theta \tag{16}$$

Here g is between -1 and 1, and is positive for forward scattering and negative for backward scattering. The asymmetry parameter is also provided by the Lorenz-Mie scattering code.

As well as using Lorenz-Mie theory, VSTAR can make use of precalculated scattering parameters derived using other methods. Scattering from non-spherical particles can be modelled using T-matrix methods (Waterman 1971; Mishchenko 1991). Codes available from Mishchenko et al. (2002) can be used to calculate the scattering properties of particles with spheroidal or cylindrical shapes or shapes described by Chebyshev polynomials in either random or specific orientations. However, T-matrix techniques are generally limited to small size parameters and can be very slow to compute. Some examples of applications of these techniques can be found in Bailey (2007) and Bailey et al. (2008).

The aerosols that make up Titan's stratospheric haze have optical properties that can be modelled by fractal aggregrates composed of many spherical particles. Models described by Tomasko et al. (2008) give the scattering properties of the Titan aerosols including optical depth, single scattering albedo and phase function in a form suitable for use with VSTAR.

2.8 Radiative Transfer

The data on absorption and scattering derived by the methods described in sections 2.2 to 2.7 are finally combined to provide the inputs needed for solving the radiative transfer equation. VSTAR is structured in a modular way so that a number of different approaches to radiative transfer can potentially be used. However, for most of our work we have used the DISORT package (Stamnes et al. 1988). DISORT is a robust computer implementation of the discrete ordinate method for radiative transfer originally developed by Chandrasekhar (1960).

DISORT models the radiative transfer in a multiple layer medium, including the processes of absorption, multiple scattering and thermal emission, and allows a reflecting surface at the lower boundary and a direct beam source (e.g. the Sun) illuminating the top of the atmosphere.

The radiative transfer equation solved by DISORT has the form:

$$\mu \frac{dI_\nu(\tau, \mu, \phi)}{d\tau} = I_\nu(\tau, \mu, \phi) - S_\nu(\tau, \mu, \phi) \tag{17}$$

where I_ν is the monochromatic radiance (sometimes referred to as intensity or specific intensity) at frequency ν, and is a function of optical depth τ, and direction μ, ϕ, where μ is the cosine of the zenith angle, and ϕ is the azimuthal angle. The source function S_ν is given by:

$$\begin{aligned} S_\nu(\tau, \mu, \phi) = {} & \frac{\varpi(\tau)}{4\pi} \int_0^{2\pi} \int_{-1}^{1} P(\mu, \phi; \mu', \phi') I_\nu(\tau, \mu', \phi') d\mu' d\phi' \\ & + (1 - \varpi) B_\nu(T) \\ & + \frac{\varpi F_\nu}{4\pi} P(\mu, \phi; \mu_0, \phi_0) \exp{(-\tau/\mu_0)} \end{aligned} \tag{18}$$

where the first term describes scattering of radiation into the beam from other directions according to single scattering albedo ϖ and phase function $P(\mu, \phi; \mu', \phi')$, the second term is thermal emission, with $B_\nu(T)$ being the Plank function and the third term is direct illumination of the atmosphere by an external source with flux $\mu_0 F_\nu$ and direction μ_0, ϕ_0 (e.g. the Sun).

The inputs required by DISORT are the vertical optical depth ($\Delta\tau$), single scattering albedo (ϖ) and phase function moments (α^s, the coefficients of the Legendre polynomial expansion of the phase function as defined in equation 14) for each atmospheric layer. The temperature at each level is also needed for thermal emission calculations.

The values of these are obtained by summing the contributions of all relevant processes for each layer of the atmosphere at each wavelength. The combined absorption due to all molecular and atomic line processes as well as related continuum processes (sections 2.2 to 2.6) is called $\Delta\tau_{gas}$. Rayleigh scattering (section 2.7.1) contributes an optical depth $\Delta\tau_{ray}$ which is pure scattering optical depth. Each of the p modes ($p = 1$ to p_{max}) of scattering particles (section 2.7.2) provides both a scattering optical depth $\Delta\tau^p_{scatt}$ and an absorption optical depth $\Delta\tau^p_{abs}$.

The total optical depth for a layer is:

$$\Delta\tau = \Delta\tau_{gas} + \Delta\tau_{ray} + \sum_{p=1}^{p_{\max}} (\Delta\tau^p_{scatt} + \Delta\tau^p_{abs}) \tag{19}$$

The combined single scattering albedo for a layer is the scattering optical depth divided by the total optical depth so is given by:

$$\varpi = \frac{\Delta\tau_{ray} + \sum_{p=1}^{p_{\max}} \Delta\tau^p_{scatt}}{\Delta\tau} \tag{20}$$

and the combined phase function moments (α^s for $s = 0$ to s_{max}) are the phase function moments for the individual scattering components, the Rayleigh scattering (α^s_{ray}) and the p particle modes (α^{sp}), weighted according to their contribution to the scattering optical depth.

$$\alpha^s = \frac{\alpha^s_{ray} \Delta\tau_{ray} + \sum_{p=1}^{p_{\max}} \alpha^{sp} \Delta\tau^p_{scatt}}{\Delta\tau_{ray} + \sum_{p=1}^{p_{\max}} \Delta\tau^p_{scatt}} \tag{21}$$

DISORT approximates the angular distribution of the radiation field, by replacing the integral term in the source function with a sum over a number of discrete zenith angles (or streams) according to the Gaussian quadrature rule. The number of streams determines how accurately the angular distribution of radiance is calculated. For many purposes where the variation with angle is reasonably smooth, we have found 8 streams (four upward and four downward) to be adequate. However, the number of streams can be increased as necesssary to provide more accurate representation of angular structure, at the cost of increased computation time.

DISORT provides a number of outputs. In astronomical cases we are mostly interested in the upward radiance and its angular dependence at the top of the atmosphere. The radiance can be determined for any emission angle, and for any azimuth relative to the illuminating source. It is also possible to determine the radiation field at the surface of the planet or at intermediate levels in the atmosphere.

The radiative transfer equation only holds for monochromatic radiance. Thus to obtain the spectrum of a planet the radiative transfer calculation must be repeated for each wavelength, and the wavelength steps made sufficiently small to resolve the spectral lines. We normally use a set of points that are equally spaced in wavenumber, and with a spacing chosen to be just sufficient to resolve the narrowest absorption lines encountered in any layer of the model. Typically this requires several hundred thousand spectral points to be calculated.

2.9 VSTAR Operation

We can now outline the full procedure for using VSTAR to calculate the spectrum of a planet, brown dwarf or star. The first steps in the process are different depending on whether we are modelling a solar-system planet (including the Earth) or an exoplanet, brown dwarf or star.

2.9.1 First Step - Solar System case

In the solar-system planet case we start with a measured profile for the temperature and pressure as a function of height. This is available for all planets in the solar system, either from radio occultation observations, or from entry probes or other in-situ data. For Earth there are a number of “standard atmosphere” profiles available and several of these are built-in to VSTAR. Some other planets have standard atmospheres, e.g. the Venus International Reference Atmosphere (VIRA, Seiff et al. 1985)

The mixing ratios of the various gases and their distribution with altitude are also generally reasonably well known from in-situ measurement or past spectroscopic analysis. Thus for any such planet we can start with an atmospheric profile which consists of a number of layers (typically 30 to 60) with the pressure, temperature, and mixing ratios of absorbing gases specified for each layer. If clouds or aerosols are included in the model their vertical distribution is specified in terms of the aerosol optical depth at a specific reference wavelength, for each particle mode at each layer.

2.9.2 First Step - Giant Exoplanet, Brown Dwarf or Star

In these cases we don't have the direct measurements of profile and composition available for solar system planets. Once again we start from a pressure-temperature profile for the atmosphere. The other input required for the model is the elemental composition of the atmosphere. For this we normally assume either a solar composition (e.g. Grevesse, Asplund & Sauval 2007; Asplund et al. 2009; Lodders, Palme & Gail 2009) or a modified solar composition for a different metallicity.

Then for each layer of the atmosphere we use the ICE chemical equilibrium model (section 2.1) to determine the equilibrium composition of the layer in terms of molecules, atoms and ions. ICE also predicts what condensates are produced at different levels in the atmosphere, and this can be used as a guide to the addition of clouds to the model which are specified in the same way as in the solar system case.

Note that VSTAR is not an atmospheric structure model, and so cannot be used to determine structures that are self consistent with the radiative transfer (although this capability may be added in the future). Currently, therefore, we normally work from a pressure-temperature structure determined from another stellar or exoplanet atmosphere model and VSTAR is used as a spectral synthesis model.

2.9.3 Second Step - Computing Layer Absorption and Scattering Properties

In either case we now have a specification of the atmospheric layers with their pressures, temperatures, chemical composition and aerosol optical depth. We now calculate for each layer at each modelled wavelength (typically there are several hundred thousand wavelength points) the absorption and scattering properties. For line absorption this involves calculating the line profiles of all the spectral lines of all relevant species that fall within the wavelength range of the model (including lines outside the range where the far wing contribution may be significant) and adding their contributions into the gas optical depth of the layer.

For particle scattering (clouds and aerosols - section 2.7.2) there are two options. Lorenz-Mie theory can be used directly to calculate the scattering properties of each particle mode at each layer for a set of wavelengths. These values are then spline interpolated to provide data for each individual wavelength point. Alternatively precalculated scattering properties can be used and interpolated in the same way.

2.9.4 Third Step - Radiative Transfer Solution

The next step is to combine the absoprtion and scattering properties of each layer as described in section 2.8 to provide the inputs needed for DISORT, and perform the radiative transfer solution for each wavelength point. At this stage we specify the boundary conditions, which can include a reflecting surface at the base of the atmosphere, and an illuminating source (the Sun or another star) at a specified zenith angle.

VSTAR can calculate a number of different types of spectra. In the case of a solar system planet we are ususally interested in the spectrum of the radiance at a specific point on the planet's disk, or the radiance factor (I/F) if we are looking at reflected solar light. For a star we generally want the flux spectrum (the radiance integrated over all angles) which is equivalent to what would be seen from an unresolved star at a large distance. However, the angular dependence of the radiance also allows the investigation of limb darkening of a star. VSTAR can also calculate the transmission spectrum from the top of the atmosphere to the surface. This is used in particular for the Earth atmosphere case where such data can be used to model telluric corrections to astronomical spectra (Bailey et al. 2007).

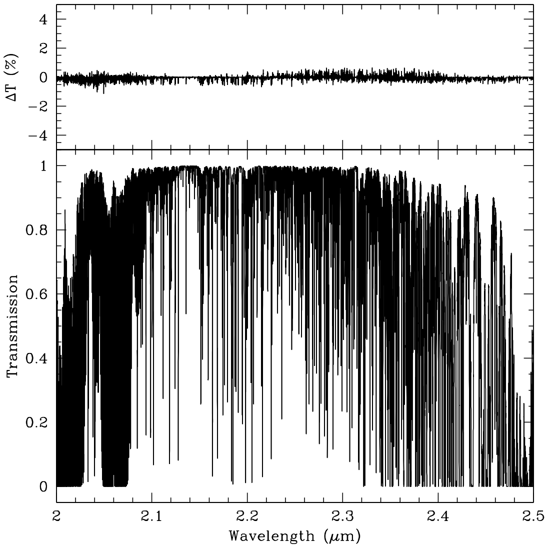

Figure 3. Comparison of Earth atmosphere zenith transmission calculated with VSTAR and RFM in the 2-2.5 μm window. Lower panel — Transmission calculated with VSTAR. Upper panel — Percentage difference (VSTAR − RFM).

3 TESTS OF VSTAR - COMPARISON WITH OTHER MODELS

We have tested VSTAR by comparing its predictions with a number of other models.

3.1 Comparison with RFM (Reference Forward Model)

The Reference Forward Model (RFM)[4] is a line-by-line model for the Earth atmosphere developed at Oxford University for the MIPAS instrument project on the Envisat satellite. RFM is itself a development of the earlier GENLN2 model (Edwards 1992). RFM has been included in a number of intercomparison studies of Earth atmosphere radiative transfer codes (Tjemkes et al. 2003; Saunders et al. 2007).

---

[4] http://www.atm.ox.ac.uk/RFM/

We compared VSTAR with RFM (version 4.25) by using both codes to calculate the Earth atmosphere transmission spectrum at the zenith in the 2 to 2.5 μm wavelength region. The atmospheric profile was the standard mid-latitude summer atmosphere taken from the RFM website. Absorption due to H_2O, CO_2, O_3, N_2O, CO, CH_4 and O_2 were included in the models with line data taken from the HITRAN 2000 database (the version of HITRAN supported by RFM).

The transmission spectrum from VSTAR and the percentage difference between transmission calculated by RFM and VSTAR are shown in figure 3. The mean difference (VSTAR − RFM) in transmission is −0.05%, and the RMS difference is 0.09%. There is no significant trend in the differences with wavelength. These results are basically a test of the line-by-line absorption calculations and show the two models are in good agreement. Residual differences between the two codes appear to be due to differences in the line shape model used, and to differences in the way layer properties are interpolated from the levels listed in the atmospheric profile.

3.2 Radiative Transfer Benchmarks

We have used VSTAR to reproduce a number of benchmark problems in radiative transfer described by Garcia & Siewert (1985). The first problem considered is a uniform Mie scattering atmosphere containing spherical particles with size parameter 2 and index of refraction 1.33. The atmosphere has a total optical depth $\tau = 1$, and the single scattering albedo $\varpi = 0.95$. The atmosphere is illuminated by a source at a zenith angle of 60 degrees and has a non-reflecting surface at its base. The problem was implemented using VSTAR's own Mie scattering code to calculate the phase function, and the results for the top of atmosphere upward radiances and bottom of atmosphere downward radiances at an azimuth of zero are given in table 4, and compared with the results summed from the fourier series coefficients given in Garcia & Siewert (1985). The VSTAR results, calculated with 16 streams in DISORT, agree with the Garcia & Siewert (1985) results to five significant figures in all cases, and at over half the zenith angles agree to within ±1 in the sixth figure. Similar agreement is found for results at other azimuths and optical depths.

Another problem we have calculated with VSTAR is one of the test problems posed by the Radiation Commission of the International Association of Meteorology and Atmospheric Physics (Lenoble 1977). This involves an atmosphere with $\tau = 1$, $\varpi = 0.9$ with a "Haze L" size distribution of scattering particles as defined by Lenoble (1977). The atmosphere is illuminated by a source at a zenith angle of 60 degrees. This problem has a more complex phase function, and with 16 DISORT streams the benchmark results in Garcia & Siewert (1985) are only matched to an accuracy of ∼1 per cent. However, increasing the number of DISORT streams to 64 produces results that agree with the Garcia & Siewert (1985) results to ±1 in the sixth significant figure for the upward radiances at the top of the atmosphere.

Table 4. Radiances for Mie scattering benchmark problem compared with values from Garcia & Siewert (1985). Positive values of μ are upward radiances at the top of the atmosphere and negative values are downward radiances at the bottom of the atmosphere, both for an azimuth of zero relative to the illuminating source.

$\mu = coszd$	VSTAR	Garcia & Siewert	Difference
1.0	0.0476802	0.0476807	−0.0000005
0.9	0.1072616	0.1072618	−0.0000002
0.8	0.162275	0.162274	0.000001
0.7	0.228132	0.228131	0.000001
0.6	0.308466	0.308464	0.000002
0.5	0.406536	0.406534	0.000002
0.4	0.525328	0.525326	0.000002
0.3	0.666624	0.666621	0.000003
0.2	0.828749	0.828746	0.000003
0.1	1.004042	1.004041	0.000001
−0.1	0.466472	0.466478	−0.000006
−0.2	0.578557	0.578561	−0.000004
−0.3	0.653528	0.653530	−0.000002
−0.4	0.682601	0.682601	0.000000
−0.5	0.674533	0.674533	0.000000
−0.6	0.637904	0.637903	0.000001
−0.7	0.578009	0.578008	0.000001
−0.8	0.496937	0.496936	0.000001
−0.9	0.391880	0.391879	0.000001
−1.0	0.197933	0.197932	0.000001

3.3 Comparison with MARCS

The MARCS stellar atmosphere code (Gustafsson et al. 2008) is a good choice for a comparison with VSTAR, since it uses modern abundances and opacities, similar to those used in VSTAR, and has been used to generate a large grid of model atmospheres with detailed information available on the model structure. The comparison shown here is for a plane parallel model with $T_{\rm eff} = 2500$ K, g = 1000 m s^{-2} ($\log g = 5$ in c.g.s units), and solar metallicity. To make the comparison we take the temperature as a function of gas pressure from the MARCS model, and use this as the input for calculating an equivalent VSTAR model.

Molecular species included in the VSTAR model were: H_2O (BT2), CO, CaH, MgH, FeH, CrH, TiO and VO. Lines of alkali metals were taken from VALD (Piskunov et al. 1995; Kupka et al. 1999), and other atomic species were from the Kurucz line lists.

Figure 4 shows some comparisons of data from MARCS and VSTAR. These include the height above the lowest level modelled (determined from hydrostatic balance), and the mixing ratios of several important species. On these plots crosses are the values from MARCS and the lines are the values from VSTAR. In most cases the agreement is excellence. The behaviour for TiO is however quite different in the cooler layers. This is because the VSTAR chemical model includes condensate formation, whereas MARCS only includes gas phase chemistry. Small differences in the CO and H_2O mixing ratios arise from the same cause. The difference in TiO does not have much effect on the strength of the TiO bands in the spectrum as these are mostly formed at deeper levels.

The flux spectrum from VSTAR is compared with that from MARCS in the bottom right panel of figure 4. The

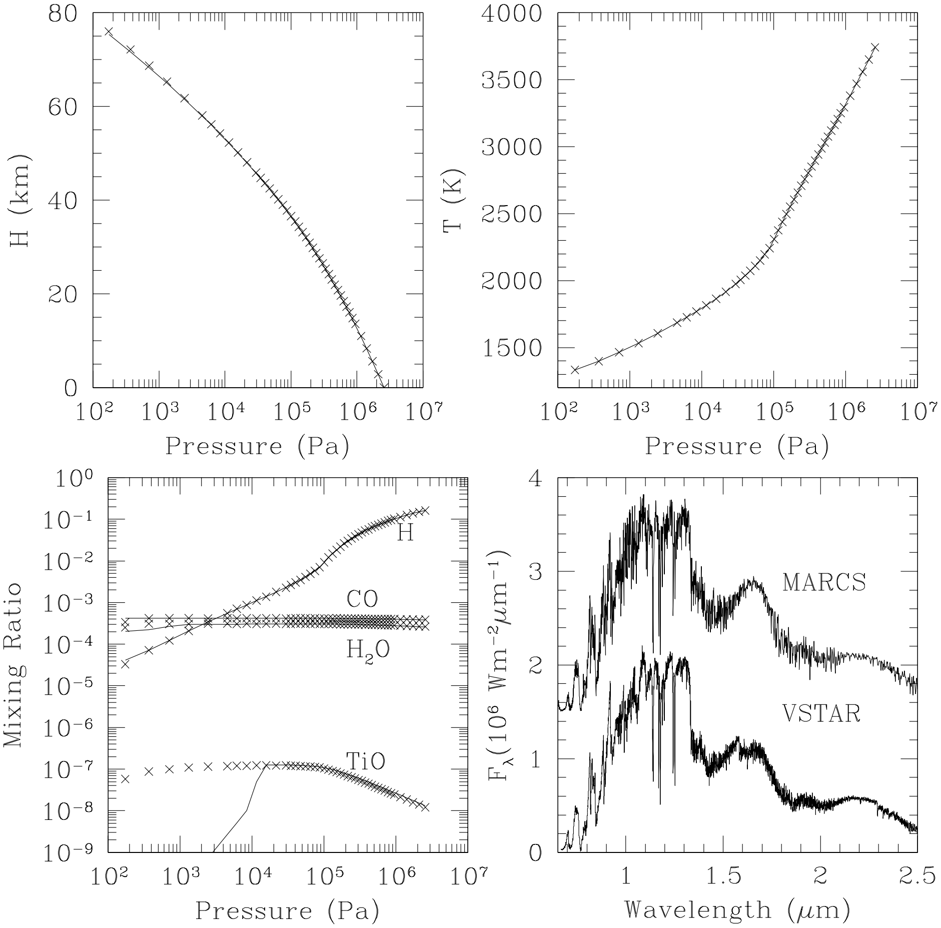

Figure 4. Comparison of MARCS and VSTAR for a stellar atmosphere model with $T_{\rm eff} = 2500$ K, $\log g = 5$ and solar metallicity. The height, temperature and mixing ratios of several important species are plotted as a function of gas pressure. On these plots crosses are the values from MARCS, and the line shows the values from VSTAR (only the temperature profile is taken from the MARCS model. All other quantities are calculated independently by VSTAR and MARCS). The flux spectra from MARCS and VSTAR are shown in the bottom right panel, with the MARCS data offset by 1.5 $\times 10^6$.

fluxes provided with MARCS are described as "rough estimates of the surface fluxes" and "are NOT synthetic spectra". Nevertheless it is clear that the values of the fluxes are very similar and the same absorption fetaures are present in both spectra at similar depths. A comparison of similar models with observations of an M dwarf spectrum are presented later.

4 COMPARISON WITH OBSERVATIONS

In this section we present a brief comparison of VSTAR models with observed spectra for a range of objects. Full details on these and other results will be given elsewhere, but they are presented here to show the wide range of astronomical objects that can be successfully modelled using VSTAR. The spectra of solar system objects are from our own observations with the Anglo-Australian 3.9m telescope at Siding Spring observatory, and its IRIS2 instrument (Tinney et al. 2004), and from the NIFS instrument (McGregor et al. 2003) on the Gemini North 8m telescope at Mauna Kea Hawaii. The brown dwarf and stellar spectra are taken from the NASA Infrared Telescope Facility (IRTF) spectral library (Cushing et al. 2005; Rayner et al. 2009) and are taken with the SpeX instrument on IRTF at a resolving power of R∼2000.

The spectra considered here are all in the near-infrared spectral region (1 – 2.5 μm). For late type dwarfs this is where the flux peaks, and for spectroscopy of planets, this is a region containing many interesting rovibrational molecular bands. While this is the wavelength region VSTAR has normally been applied to, there is nothing inherent in VSTAR that restricts it to this region. VSTAR should, in principle, be usable from UV to microwave wavelengths.

4.1 Solar System Objects

Figure 5 shows a number of comparisons of observed spectra with VSTAR models for solar system atmospheres. The Earth atmosphere transmission comparison (top left panel) is described in more detail in Bailey et al. (2007) and Bailey et al. (2008) and uses the observed spectrum at a re-

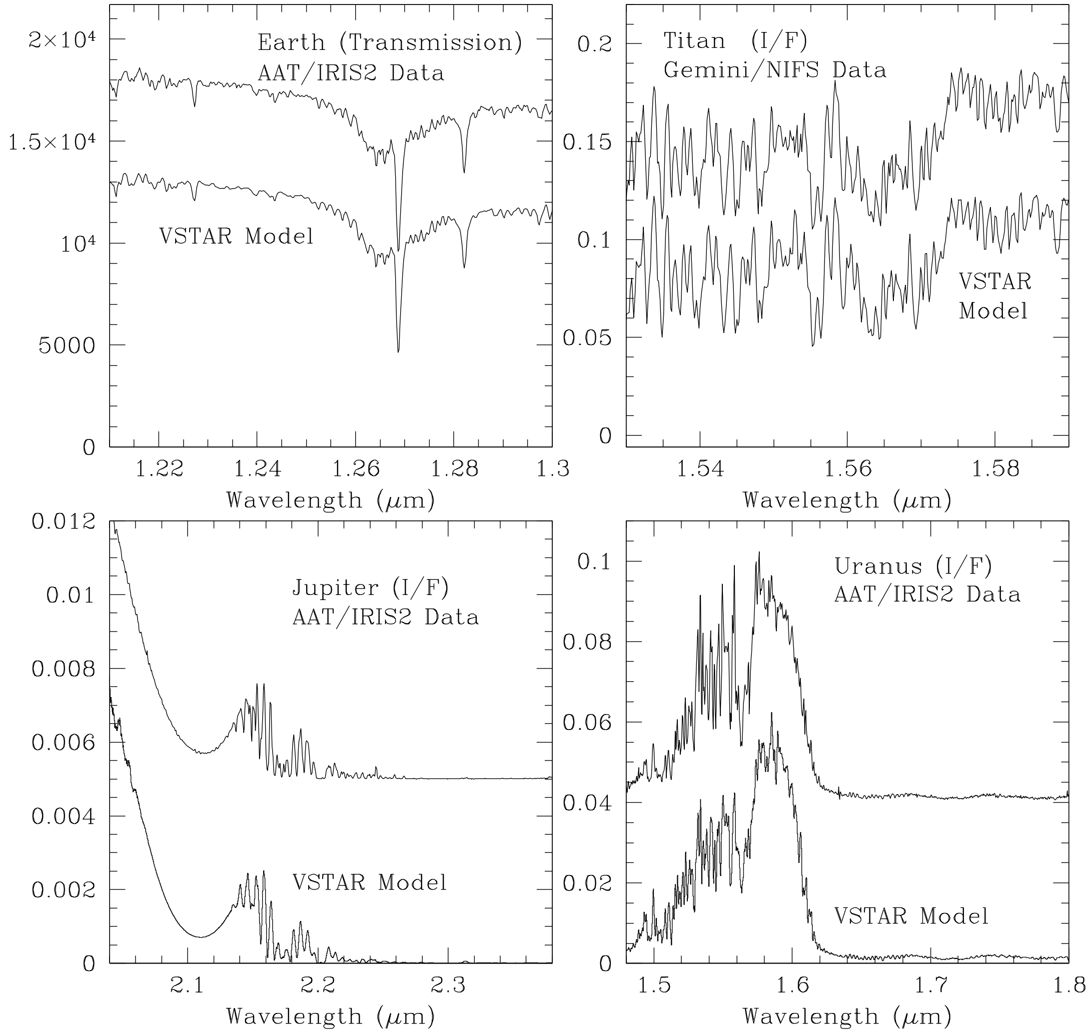

Figure 5. Comparison of observed spectrum of solar system objects with VSTAR model spectra. At top left is shown the spectrum of a G2V star seen through the Earth's atmosphere in the region of the O_2 a-X absorption band, compared with a VSTAR model for a solar spectrum with Earth atmospheric transmission applied. The other three panels show observed reflectance spectra of Titan, Jupiter and Uranus compared with VSTAR models. The observed spectrum in each case is offset upwards relative to the model spectrum.

solving power of R ($=\lambda/\Delta\lambda$) $\sim$ 2400 of the G5V star BS 996 with the 3.9m Anglo-Australian Telescope (AAT) and its IRIS2 instrument. This spectrum is compared with a model of a solar spectrum as seen through a modelled Earth atmosphere transmission spectrum calculated using VSTAR. Of the spectral features only that near 1.28 μm is a stellar line. Other features are atmospheric absorptions of O_2, CO_2 and H_2O, with the strongest feature being the O_2 a-X band at 1.27 μm and its associated collision induced absorption. The data and model agree to better than 1%.

The bottom left panel shows the reflected light spectrum of Jupiter in the near-infrared K band (2.04 – 2.38 μm) also observed with the AAT and IRIS2. The VSTAR model used here is described in more detail in Kedziora-Chudczer & Bailey (2011). The absoprtion features present in this spectral region are due to methane, and to the collision induced absoprtion of H_2-H_2 (see section 2.6.2), with the latter producing the broad smooth feature centred on 2.11 μm. Stratospheric and tropospheric clouds are included in the model with the details of the cloud properties and optical depths given in Kedziora-Chudczer & Bailey (2011).

The right hand panels of figure 5 show spectra of Titan and Uranus in the spectral region covering the 1.55 μm methane "window" that lies between strong methane absoprtion bands. Modelling of the spectra of these objects at this wavelength using line-by-line methods has only become possible very recently with the availability of the latest labo-

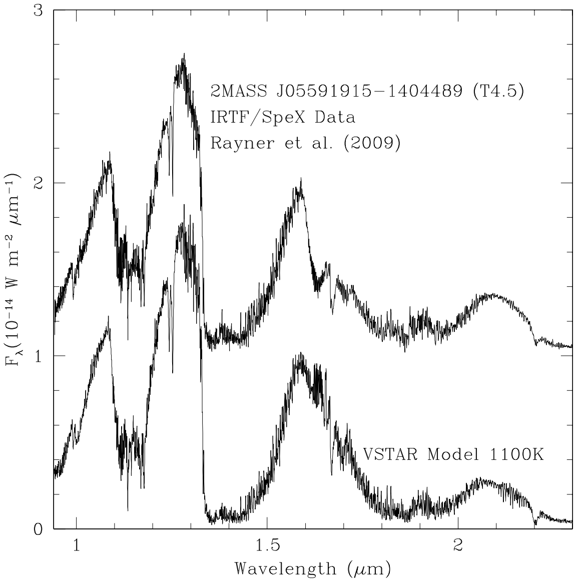

Figure 6. Comparison of observed spectrum of the T4.5 dwarf 2MASS J055591915−1404489 with a model spectrum calculated with VSTAR for $T_{\rm eff} = 1100$K and $\log g = 5$. The observed spectrum is offset from the model upwards by 1 ($\times$ 10^{-14})

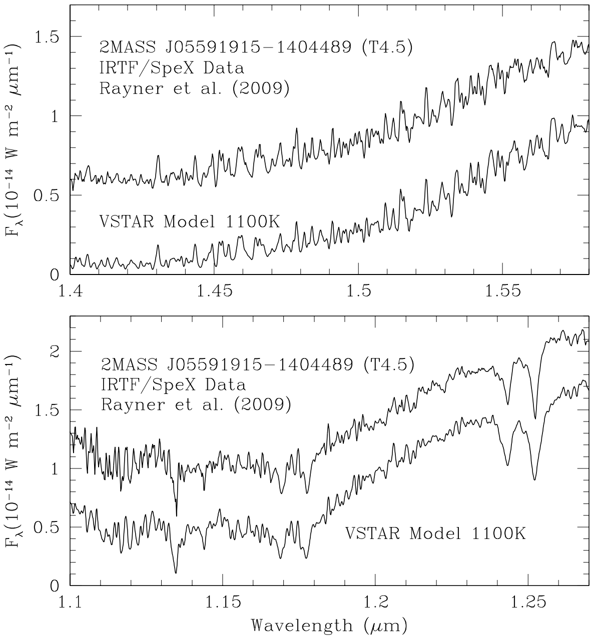

Figure 7. Expanded view of two sections of the spectrum shown in figure 6. The observed spectra are offset from the model upwards by 0.5 ($\times$ 10^{-14})

ratory spectral line data for methane as described in section 2.2.6, in particular the data of Wang et al. (2011). The Titan spectrum was obtained with the Near Infrared Integral Field Spectrometer (NIFS) on the Gemini North 8m telescope, and the data and VSTAR model are described more fully by Bailey, Ahlsved & Meadows (2011). The absorption lines in this region are mostly weak lines of CH_4, but there are also lines of CH_3D and CO. A model for Titan's aerosols based on that of Tomasko et al. (2008) is also used in this analysis. The models enabled Titan's D/H ratio and CO abundance to be determined as described in Bailey et al. (2011).

The Uranus comparison in the lower right panel uses data from IRIS2 on the AAT. The VSTAR model spectrum is calculated from the new low temperature methane line data as described in section 2.2.6. The model includes clouds with a mean particle size of 1 μm, and with the main cloud layers being at 2 – 3 bars and at 6 – 10 bars, which is similar to cloud distributions derived by Sromovsky, Irwin & Fry (2006) and Irwin, Teanby & Davis (2007).

While not shown here VSTAR has also been used successfully to model the spectra of other solar system planets. VSTAR models for the Venus night side are used in the analyses described by Bailey (2009) and Cotton et al. (2011)

4.2 Brown Dwarf

Figure 6 shows an observed spectrum of the T4.5 dwarf 2MASS J05591915−1404489 taken from the IRTF spectral library (Cushing, Rayner & Vacca 2005; Rayner, Cushing & Vacca 2009) compared with a VSTAR model spectrum. The VSTAR spectra used for this comparison are based on brown dwarf model P-T structures taken from Figures 8 and 9 of Burrows et al. (2006). The VSTAR models included molecular absorption due to H_2O (BT2), CO, CH_4, CaH, MgH, CrH, FeH, TiH. Lines of alkali metals are included from VALD (Piskunov et al. 1995; Kupka et al. 1999). The far wings of very strong sodium and potassium lines in the visible have a significant effect on the shape of brown dwarf spectra in the 1 μm region. We used a χ factor model for the far wing shapes of these lines with an exponentially decrease between 500 and 7500 cm^{-1} from the line centre, with the parameters adjusted to provide a good match to the data. More physically based models for the far wing shapes of alkali metal lines are described by Burrows & Volobuyev (2003) and Allard et al. (2003).

A number of models were tried with different temperatures and gravities, and best agreement with the data was found for a model with $T_{\rm eff} = 1100$ K, g = 1000 m s^{-2} ($\log g$ = 5 in c.g.s. units) and solar metallicity. This is in reasonable agreement with other results for this object.Stephens et al. (2009) find $T_{\rm eff} = 1200$ K, $\log g = 4.5$ while del Burgo et al. (2009) find $T_{\rm eff} = 1002$ K, $\log g = 4.9$ using high resolution spectra.

The model spectrum agrees well with the observed spectrum except in the wavelength region from around 1.6 – 1.7 μm. As discused in section 2.2.6, the methane line lists currently available do not include hot bands in this region and therefore underestimate the total absorption, and incorrectly model the observed structure. This problem exists with all models for T-dwarf spectra. There is also a discrepancy between the model and observations in the 2.1 μm region where the model is slightly too low.

In other wavelength regions, where methane absorption

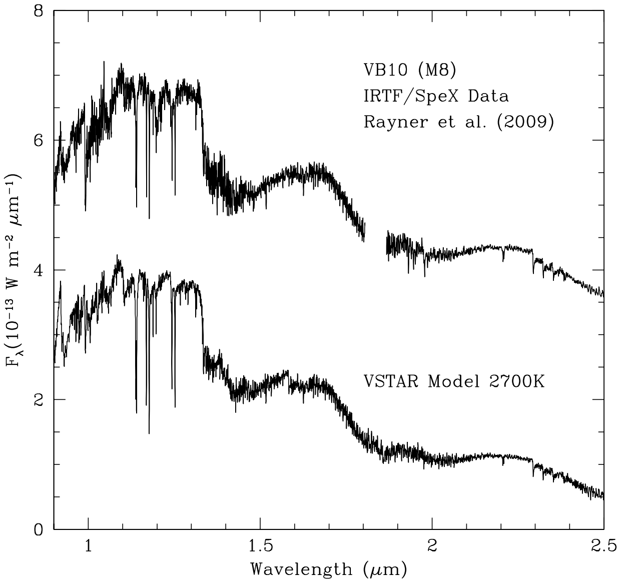

Figure 8. Comparison of observed spectrum of the M8 dwarf VB10 with a model spectrum calculated with VSTAR using a MARCS model structure for $T_{\rm eff} = 2700$K and $\log g = 5$. The observed spectrum is offset from the model upwards by 3 ($\times$ 10^{-13})

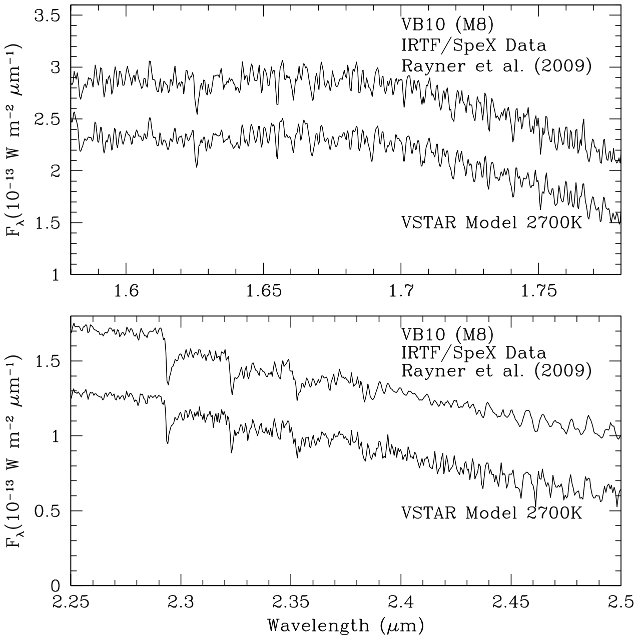

Figure 9. Expanded view of two sections of the spectrum shown in figure 8. The observed spectra are offset from the model upwards by 0.4 ($\times$ 10^{-13}). The upper panel shows primarily absorption in the E-A band of FeH. The lower panel shows absorption due to CO and H_2O.

.

is not significant, the agreement between model and observations is excellent. What might, at first sight, appear to be noise on the spectra, is in fact spectral structure due to many absorption lines. This is apparent from figure 7 where two wavelength regions (1.1 – 1.27 μm and 1.4 – 1.58 μm) are shown on an expanded scale.

The model used here did not include dust absorption and scattering. This is acceptable for objects as late as T4.5. For earlier type brown dwarfs, and in particular the L-dwarf class, the effects of dust are important. While VSTAR is quite capable of modelling the radiative effects of dust in such systems, there are currently considerable diferences in the assumptions about dust properties used in different models. Some models use large ($\sim$100 μm) dust particles (Burrows et al. 2006) while others use small (sub-μm) particles (Allard et al. 2001). For the purposes of this paper we have avoided the extra complexity of dusty brown dwarf models.

Our models also assume equilibrium chemistry. Some brown dwarf models include a non-equlibrium treatment of the chemistry of some species such as CH_4, CO and H_2O (Saumon et al. 2003; Stephens et al. 2009) which allows for the effects of vertical mixing in the atmosphere. While this could be implemented as a modification to our chemical model we have not done so for the results presented here. The effects on the near-IR spectrum appear to be small (Hubeny & Burrows 2007) with more significant effects at 4 – 14 μm wavelengths.

4.3 M Dwarf

Figure 8 shows an observed spectrum of the M8 dwarf VB10 (Gl 752B) taken from the IRTF spectral library (Cushing, Rayner & Vacca 2005; Rayner, Cushing & Vacca 2009) compared with a model spectrum calculated with VSTAR. The model structure was taken from the MARCS grid of model atmospheres (Gustafsson et al. 2008) and is a model for $T_{\rm eff} = 2700$ K, g = 1000 m s^{-2} ($\log g = 5$ in c.g.s. units) and solar metallicity. In other respects the model is similar to that described in section 3.3. A number of different effective temperatures were tested with the 2700 K model providing the best match to the observed spectrum.

Figure 9 shows expanded views of two regions of the spectrum. The upper panel shows the 1.58 – 1.78 μm region. This is dominated by absorption lines in the E-A band of FeH, which are included in our model using the line list of Hargreaves et al. (2010). This band is essential to get a good model of the spectrum in this region. However, including this line list results in a small step in the modelled spectrum at 1.582 μm (visible in figure 8) which is the shortest wavelength included in this list. This step is not seen in the observed spectrum, and suggests that there is more FeH absorption at shorter wavelengths that should be included. The lower panel of figure 9 is 2.25 – 2.5 μm region showing that the model does a good job of representing the detailed structure of the CO and H_2O bands in this region. As for the brown dwarf case we have used a dust free model. It is quite possible that dust is present in such a late type M dwarf, and its inclusion might change our conclusions about the best fitting effective temperature.

The upper limit on the layer temperature for modelling stellar atmospheres using VSTAR is currently 6000 K set by the use of data from the JANAF tables in our chemical model. Since a model usually requires a range of layer temperatures extending to about a factor of two above and below the effective temperature of the star being modelled, the maximum effective temperature is around 3000 K.

5 CONCLUSIONS

We have desribed the techniques used in the VSTAR code to calculate model spectra for objects including solar-system planets, brown dwarfs and M dwarfs. While there are other codes used for modelling the spectra of these objects, VSTAR has a number of unique features.

- It is capable of being used for a very wide range of objects, ranging from the coolest solar system planets (Uranus with layer temepratures down to 60 K) to stars with layer temperatures up to 6000 K.
- It has been tested by comparison with both the Earth atmosphere radiative transfer code (RFM) and a stellar atmosphere code (MARCS).
- Not only is a rigorous approach to radiative transfer used, but this has been tested against radiative transfer benchmarks and shown to be accurate to levels of 10^{-5} to 10^{-6}.

An obvious application of VSTAR is to the modelling of exoplanet spectra. VSTAR has the proven ability to model both cool planets in our own solar system, and hotter objects such as brown dwarfs and M dwarfs, and thus covers the full temperature range expected to be encountered in exoplanets. The full treatment of the angular dependence of scattering incorporated in VSTAR means that it can be used to predict the phase dependence of an exoplanet spectrum around its orbital cycle.

Work is currently in progress on extending VSTAR to include polarized radiative transfer. The phase variation of polarization can potentially provide important information about an exoplanet's atmosphere or surface (Bailey 2007; Stam 2008; Zugger et al. 2010)

Acknowledgments

Based on observations obtained at the Gemini Observatory which is operated by the Association of Universities for Research in Astronomy, Inc. under a cooperative agreement with the NSF on behalf of the Gemini partnership: the National Science Foundation (United States), the Science and Technology Facilities Council (United Kingdom), the National Research Council (Canada), CONICYT (Chile), the Australian Research Council (Australia), Ministerio da Cienca e Tecnologia (Brazil) and Ministerio de Ciencia, Tecnologia e Innovacion Productiva (Argentina). The Titan observations were obtained as part of the system verification of the NIFS instrument under program GN-2006A-SV-128. We thank the staff of the Australian Astronomical Observatory for assistance in obtaining observations with the Anglo-Australian Telescope.

REFERENCES

Albert, S., Bauerecker, S., Boudon, V., Brown, L.R., Champion, J.-P., Loete, M., Nikitin, A. & Quack, M., 2009, Chem. Phys., 356, 131.

Allard, F., Hauschildt, P.H., Schwenke, D., 2000, ApJ, 540, 1005.

Allard, F., Hauschildt, P.H., Alexander, D.R., Tamanai, A., Schweitzer, A., 2001, ApJ, 556, 357.

Allard, N.F., Allard, F., Hauschildt, P.H., Kielkopf, J.F., Machin, L., 2003, A&A, 411, 473.

Asplund, M., Grevesse, N., Sauval, A.J., Scott, P., 2009, ARA&A, 47, 481.

Barber, R.J., Tennyson, J., Harris, G.J., Tolchenov, R.N., 2006, MNRAS, 368, 1087.

Bailey, J., 2006, in Forget, F. et al., (eds) Proceedings Mars Atmosphere Modelling and Observations Workshop, Granada, 148, Laboratoire Meteorologie Dynamique, Paris.

Bailey, J., 2007, Astrobiology, 7, 320.

Bailey, J., Simpson, A., Crisp, D., 2007, PASP, 119, 228.

Bailey, J., Ulanowski, Z., Lucas, P.W., Hough, J.H., Hirst, E., Tamura, M., 2008a, MNRAS, 386, 1016.

Bailey, J., Meadows, V.S., Chamberlain, S., Crisp, D., 2008b, Icarus, 197, 247.

Bailey, J., 2009, Icarus, 201, 444.

Bailey, J., Ahlsved, L., Meadows, V.S., 2011, Icarus, 213, 218.

Barin, I., 1995, Thermochemical Data of Pure Substances (3rd ed); VCH-Verlag, Weinheim

Barman, T.S., Hauschildt, P.H., Allard, F., 2001, ApJ, 556, 885.

Bell, K.L., 1980, J. Phys. B, 13, 1859.

Bell, K.L. & Berrington, K.A., 1987, J. Phys. B, 20, 801.

Borysow, A., 2002, A&A, 390, 779.

Borysow, A. & Frommhold, L., 1989, ApJ, 341, 549.

Borysow, A., Frommhold, L., Massimo, M., 1989, ApJ, 336, 495.

Borysow, A., Jørgensen, U.G., Zheng, C., 1997, A&A, 324, 185.

Borysow, A., Jørgensen, U.G., Fu, Y., 2001, J. Quant. Spectrosc. Radiat. Trans., 2001, 68, 235.

Borysov, A., Champion, J.P., Jørgensen, U.G., Wenger, C., 2002, Mol. Phys., 100, 3585.

Boudon, V., Rey, M., Loete, M., 2006, J. Quant. Spectrosc. Radiat. Trans., 98, 394.

Brown, L.R., 2005, J. Quant. Spectrosc. Radiat. Trans., 96, 251.

Brown, L.R. & Peterson, D.B., 1994, J. Mol. Spectrsoc., 168, 593.

Burch, D.E., Singleton, E.B., Williams, D., 1962, Appl. Opt., 1, 359.

Burch, D.E., Gryvnak, D.A., Patty, R.R., Bartky, C.E., 1969, J. Opt. Soc. Am., 59, 267.

Burrows, A. & Sharp, C.M., 1999, ApJ, 512, 843.

Burrows, A., Volobuyev, M., 2003, ApJ, 583, 985.

Burrows, A., Ram, R.S., Bernath, P., Sharp, C.M., Milsom, J.A., 2002, ApJ, 577, 986.

Burrows, A., Sudarsky, D., Hubeny, I., 2003, ApJ, 588, 1121.

Burrows, A., Dulick, M., Bauschlicher, C.W., Bernath, P.F., Ram, R.S., Sharp, C.M., Milson, J.A., 2005, ApJ, 624, 988.

Burrows, A., Sudarsky, D., Hubeny, I., 2006, ApJ, 640, 1063.

Cahoy, K.L., Marley, M.S., Fortney, J.J., 2010, ApJ, 724, 189.

Campargue, A., Wang, L. Kassi, S., Masát, M., Ondřej., V., 2010, J. Quant. Spectrosc. Radiat. Trans., 111, 1141.

Chandrasekhar, S., 1960, Radiative Transfer, Dover, New York.

Chase, M.W., 1998, NIST-JANAF Thermochemical Tables, J. Phys. Chem. Ref. Data Monograph No. 9.

Cotton, D.V., Bailey, J., Crisp, D., Meadows, V.S., 2011, Icarus, in press.

Cox, A.N., 2000, Allen's Astrophysical Quantities, 4th edition, Springer-Verlag, New York.

Cushing, M.C., Rayner, J.T., Vacca, W.D., 2005, ApJ, 623, 1115.

Cushing, M.C. et al., 2006, ApJ, 648, 614.

Dalgarno, A. & Williams, D.A., 1962, ApJ, 136, 690.

de Bergh, C. et al., 2011, Planet. Space Sci., in press doi:10.1016/j.pss.2011.05.003.

Delaye, C., Hartmann, J.-M., Taine, J., 1989, Appl. Opt., 28, 5080.

del Burgo, C., Martin, E.L., Zapatero Osorio, M.R., Hauschildt, P.H., 2009, A&A, 501, 1059.

Dulick, M., Bauschlicher, C.W., Burrows, A., Sharp, C.M., Ram, R.S., Bernath, P., 2003, ApJ, 594, 651.

Edwards, D.P., 1992, NCAR Technical Note NCAR/TN-367+STR, National Centre for Atmospheric Research, Boulder, Colorado.

Fischer, J., Gamache, R.R., Goldman, A., Rothman, L.S., Perrin, A., 2003, J. Quant. Spectrosc. Radiat. Trans., 82, 401.

Fortney, J.J., Marley, M.S., Lodders, K., Saumon, D., Freedman, R., 2005, ApJ, 627, L69.

Freedman, R.S., Marley, M.S., Lodders, K., 2008, ApJS, 174, 504.

Gamache, R.R., Lynch, R., Brown, L.R., 1996, J. Quant. Spectrosc. Radiat. Trans., 56, 471.

Garcia, R.D.M. & Siewert, C.E., 1985, Transport Theory and Statistical Physics, 14, 437.

Gao, B., Kassi, S., Campargue, A., 2009, J. Mol. Spectrosc., 253, 55.

Goody, R., West, R., Chen, L., Crisp, D., 1989, J. Quant. Spetrosc. Radiat. Trans., 42, 539.

Goorvitch, D., 1994, ApJS, 95, 535.

Gray, D.F., 2005, The Observation and Analysis of Stellar Photospheres (3rd ed); Cambridge Univ. Press, Cambridge

Grevesse, N., Asplund, M., Sauval, A.J., 2007, Space Sci. Rev., 130, 115.

Gustaffson, B., Edvadrsson, B., Eriksson, K., Jørgensen, U.G., Nordlund, A., Plez, B., 2008, A&A, 486, 951.

Hansen, J.E. & Travis, L.D., 1974, Space Sci. Rev., 16, 527.

Hargreaves, R.J., Hinkle, K.H., Bauschlicher, C.W., Wende, S., Seifahrt, A., Bernath, P.F., 2010, AJ, 140, 919.

Harris, G.J., Tennyson, J., Kaminsky, B.M., Pavlenko, Ya. V., Jones, H.R.A., 2006, MNRAS, 367, 400.

Hartmann, J.M., Rosenmann, L., Perrin, M.Y., Taine, J., 1988, Appl. Opt., 27, 3063.

Henyey, L.G. & Greenstein, J.L., 1941, ApJ, 93, 70.

Homeier, D., Hauschildt, P.H., Allard, F., 2003, in Hubeny, I., Mihalas, D., Werner, K. (eds) Stellar Atmosphere Modelling, ASP Conf. Series., 288, p357, Astronomical Society of Pacific, San Francisco.

Hubeny, I., Burrows, A., 2007, ApJ, 669, 1248.

Humlicek, J., 1982, J. Quant. Spectrosc. radiat. Trans., 27, 437.

Irwin, A.W., 1981, ApJS, 45, 621.

Irwin, A.W., 1988, A&AS, 74, 145.

Irwin, P.G.J., Sromovsky, L.A., Strong, E.K., Sihra, K., Teanby, N.A., Bowles, N., Calcutt, S.B., Remedios, J.J., 2006, Icarus, 181, 309.

Irwin, P.G.J., Teanby, N.A., Davis, G.R., 2007, ApJ, 665, L71.

Jacquinet-Husson, N. et al., 2008, J. Quant. Spectrosc. Radiat. Trans., 109, 1043.

Jones, H.R.A., Pavlenko, Y., Viti, S., Tennyson, J., 2003, in Brown, A., Harper, G.M. & Ayres, T.R. (eds) The future of Cool-Star Astrophysics: 12th Cambridge Workshop on Cool Stars, Stellar Systems, and the Sun, p899, Univ. of Colorado.

Jørgensen, U.G., 1994, A&A, 284, 179.

Jørgensen, U.G., Larsson, M., 1990, A&A, 238, 424.

Jørgensen, U.G., Larsson, M., Iwamae, A., Yu, B., 1996, A&A, 315, 204.

Jørgensen, U.G., Jensen, P., Sørensen, G.O., Aringer, B., 2001, A&A, 372, 249.

Karkoschka, E. & Tomasko, M.G., 2010, Icarus, 205, 674.

Kedziora-Chudczer, L., and Bailey, J., 2011, MNRAS, 414, 1483.

Kupka, F., Piskunov, N., Ryabchiokva, T.A., Stempels, H.C., Weiss, W.W., 1999, A&AS, 138, 119.

Kurucz, R., 1970, Atlas: a Computer Program for Calculating Model Stellar Atmospheres, SAO Special Report 309, Smithsonian Astrophysical Observatory, Cambridge, Mass.

Kurucz, R., 2005, Mem S. A. It. Suppl. 8, 86.

Kurucz, R. & Avrett, E.H., 1981, Solar Spectrum Synthesis I. A sample atlas from 224 to 300nm, SAO Special Report 391, Smithsonian Astrophysical Observatory, Cambridge, Mass.

Laraia, A.L., Gamache, R.R., Lamouroux, J., Gordon, I.E., Rothman, L.S., 2011, Icarus, 215, 391.

Lenoble, J. (Ed), Standard procedures to Compute Atmopsheric Radiative Transfer, National Centre for Atmospheric Research, Boulder, Colorado.

Liou, K.N., 2002, An Introduction to Atmospheric Radiation, Academic Press, San Diego

Lodders, K., 1999, J. Phys. Chem. Ref. Data, 28, 1705.

Lodders, K., 2004, J. Phys. Chem. Ref. Data, 33. 357.

Lodders, K. & Fegley, B., 2002, Icarus, 155, 393.

Lodders, K., Palme, H., Gail, H.-P., 2009, arXiv:1001.4635.

Marcy, G.W., Butler, R.P., Williams, E., Bildsten, L., Graham, J.R., Ghez, A.M., Jernigan, J.G., 1997, ApJ, 481, 926.

Margolis, J.S., 1990, Appl. Opt. 29, 2295.

Marley, M.S. & McKay, 1999, Icarus, 138, 268.

Marley, M.S., Seager, S., Saumon, D., Lodders, K., Ackerman, A.S., Freedman, R.S., Fan, X., 2002, ApJ, 568, 335

Mayer, J.E. & Mayer, M.G., 1940 Statistical Mechanics, Wiley, New York.

Mayor, M. & Queloz, D., 1995, Nature, 378, 355.

McKay, C.P., Pollack, J.B., Courtin, R., 1989, Icarus, 80, 23.

McKellar, A.R.W., 1989, Icarus, 80, 361.

McGregor, P.J. et al., 2003, SPIE Proc., 4841, 1551.

Meadows, V.S., Crisp, D., 1996, J. Geophys. Res., 101, 4595.

Mishchenko, M.I., 1991, J. Opt. Soc. Am., 8, 871.

Mishchenko, M.I., Travis, L.D., Lacis, A.A., 2002, Scattering, Absorption and Emission of Light by Small Particles, Cambridge University Press, Cambridge

Mondelain, D., Kassi, S., Wang, L., Campargue, A., 2011, Phys. Chem. Chem. Phys., 13, 7985.

Nakajima, T., Oppenheimer, B.R., Kulkarni, S.R., Golimowski, D.A., Matthews, K., Durrance, S.T., 1995, Nature, 378, 463.

Nikitin, A.V. et al., 2010, J. Quant. Spectrosc. Radiat. Trans., 111, 2211.

Nikitin, A.V. et al., 2011, J. Quant. Spectrosc. Radiat. Trans., 112, 28.

Nouri, S., Orphal, J., Aroui, H., Hartmann, J.-M., 2004, J. Mol. Spectrosc., 227, 60.

Old, J.G., Gentili, K.L., Peck, E.R., 1971, J. Opt. Soc. A., 61, 89.

Oppenheimer, B.R., Kulkarni, S.R., Matthews, K., Nakajima, T., 1995, Science, 270, 1478.

Partridge, H., & Schwenke, D.W., 1997, J. Chem. Phys., 106, 4618.

Pavlenko, Ya. V., Jones, H.R.A., Lyubchik, Yu., Tennyson, J., Pinfield, D.J., 2006, A&A, 447, 709.

Peck, E.R. & Reeder, K., 1972, J. Opt. Soc. Am., 62, 950.

Perrin, M.Y. & Hartmann, J.M., 1989, J. Quant. Spectrosc. Radiat. Trans., 42, 311.

Pine, A.S., 1992, J. Chem. Phys., 97, 773.

Pine, A.S. & Gabard, T., 2003, J. Mol. Spectrosc., 217, 105.

Piskunov, N.E., Kukpa, F., Ryabchikova, T.A., Weiss, W.W., Jeffery, C.S., 1995, A&AS, 112, 525.

Plez, B., 1998, A&A, 337, 495.

Pollack, J.B., Dalton, J.B., Grinspoon, D., Wattson, R.B., Freedman, R., Crisp, D., Allen, D.A., Bezard, B., de Bergh, C., Giver, L.P., Ma, Q., Tipping, R., 1993, Icarus,103, 1.

Querci, F., Querci, M., Kunde, V.G., 1971, A&A, 15, 256.

Querci, F., Querci, M., Tsuji, T., 1974, A&A, 31, 265.

Rayner, J.T., Cushing, M.C., Vacca, W.D., 200, ApJS, 185, 289.

Régalia-Jarlot, L., Thomas, X., Von der Heyden, P., Barbe, A., 2005, J. Quant. Spectrosc. Radiat. Trans., 91, 121.

Robert, O., Hilico, J.-C., Loete, M., Champion, J.-P., Brown, L.R., 2001, J. Mol. Spectrosc., 209, 14.

Robie, R.A. & Hemingway, B.S., 1995, US Geological Survey Bull. 2131.

Rothman, L.S., Wattson, R.B., Gamache, R., Schroeder, J.W., McAnn, A., 1995, in Daintey, J.C. (ed), Atmospheric Propagation and Remote Sensing IV. SPIE Proc. 2471, 105, SPIE, Bellingham, Washington.

Rothman, L.S. et al., 1998, J. Quant. Spectrosc. Radiat. Trans., 60, 665.

Rothman, L.S. et al., 2005, J. Quant. Spectrosc. Radiat. Trans., 96, 139.

Rothman, L.S. et al., 2009, J. Quant. Spectrosc. Radiat. Trans., 110, 533.

Rothman, L.S. et al., 2010, J. Quant. Spectrosc. Radiat. Trans., 111, 2139.

Saumon, D., Marley, M.S., Lodders, K., Freedman, R.S., 2003, in Martin, E.L. (ed), "Brown Dwarfs", IAU Symp, 211, Astronomical Society of the Pacific, San Francisco, p. 345.

Saunders, R. et al., 2007, J. Geophys. Res., 112, D01S90.

Sauval, A.J. & Tatum, J.B., 1984, ApJS, 56, 193.

Schreier, F., 1992, J. Quant. Spectrosc. Radiat. Trans., 27, 437.

Schwenke, D., 1998, Faraday Discussions, 109, 321.

Schwenke, D., Partridge, H., 2000, J. Chem. Phys. 113, 129.

Seager, S., Whitney, B.A., Sasselov, D.D., 2000, ApJ, 540, 504.

Seiff, A. et al., 1985, Adv. Space Res., 5, 3.

Sharp, C.M. & Huebner, W.F., 1990, ApJ, 72, 417.

Sharp, C.M. & Burrows, A., 2007, ApJS, 168, 140.

Šimečková, M., Jacquemart, D., Rothman, L.S., Gamache, R.R., Goldman, A., 2006, J. Quant. Spectrosc. Radiat. Trans., 98, 130.

Skory, S., Weck, P.F., Stancil, P.C., Kirby, K., 2003, ApJS, 148, 599.

Smith, K.M. & Newnham, D.A., 1999, Chem. Phys. Lett., 308, 1.

Smith, K.M. & Newnham, D.A., 2000, J. Geophys. Res., 105, D6, 7383.

Sneep, M. & Ubachs, W., 2005, J. Quant. Spectrosc. Radiat. Trans., 92, 293.

Sromovsky, L.A., Irwin, P.G.J., Fry, P.M., 2006, Icarus, 182, 577.

Stam, D.M., 2008, A&A, 482, 989.

Stamnes, K., Tsay, S.C., Wiscombe, W., Jayaweera, K., 1988, Appl. Opt., 27, 2502.

Stephens, D.C. et al., 2009, ApJ, 702, 154.

Strong, K., Taylor, F.W., Calcutt, S.B., Remedios, J.J., Ballard, J., 1993, J. Quant. Spectrosc. Radiat. Trans., 50, 363.

Swain, M.R., Vasisht, G., Tinnetti, G., 2008, Nature, 452, 329.

Swain, M.R., Vasisht, G., Tinetti, G., Bouwman, J., Chen, p., Yung, Y., Deming, D., Deroo, P., 2009a, ApJL, 690, L114.

Swain, M.R. et al., 2009b, ApJ, 704, 1616.

Takano, Y. & Liou, K.-N., 1989, J. Atmos. Sci., 46, 3.

Tashkun, S.A., Perevalov, V.I., Teffo, J-L., Bykov, A.D., Lavrentieva, N.N., 2003, J. Quant. Spectrosc. Radiat. Trans., 82, 165.

Tinney, C., et al., 2004, SPIE Proc., 5492, 998.

Tjemkes, S.A. et al., 2003, J. Quant. Spectrosc. Radiat. Trans., 77, 433.

Tomasko, M.G., Doose, L., Engel, S., Dafoe, L.E., West, R., Lemmon, M., Karkoschka, E., See, C., 2008, Plan. Space Sci., 56, 669.

Tonkov, M.V. et al., 1996, Appl. Opt., 35, 4863.

Tsuji, T., 1973, A&A, 23, 411.

Tsuji, T., Ohnaka, K., Aoki, W., Nakajima, T., 1996, A&A, 308, L29.

van Vleck, J.H. & Weisskopf, V.F., 1945, Rev. Mod. Phys., 17, 227.

Vidler, M. & Tennyson, J., 2000, J. Phys. Chem., 113, 9766.

Voronin, B.A., Tennyson, J., Tolchenov, R.N., Lugovskoy, A.A., Yurchenko, S.N., 2010, MNRAS. 402. 492.

Wang, L., Kassi, S., Campargue, A., 2010, J. Quant. Spectrosc. Radiat. Trans., 111, 1130.

Wang, L., Kassi, S., Liu, A.W., Hu, S.M., Campargue, A., 2011, J. Quant. Spectrosc. Radiat. Trans., 112, 937.

Waterman, P.C., 1971, Phys. Rev. D., 3, 825.

Weck, P.F., Schweitzer, A., Stancil, P.C., Hauschildt, P.H., Kirby, K., 2003, ApJ, 582, 1059.

Wenger, C. & Champion, J.P., 1998, J. Quant. Spectrosc. Radiat. Trans., 59, 471.

Wenger, C., Champion, J.P., Boudon, V., 2008, J. Quant. Spectrosc. Radiat. Trans., 109, 2697.

Wishart, A.W., 1979, MNRAS. 187. 59P.

Young, A.T., 1981, Appl. Opt., 20, 533.

Yamamura, I., Tsuji, T., Tanabe, T., 2010, ApJ, 722, 682.

Yurchenko, S.N., Barber, R.J., Yachmenev, A., Thiel, W., Jensen, P., Tennyson, J., 2009, J. Phys. Chem., 113, 11845.

Yurchenko, S.N., Barber, R.J., Tennyson, J., 2011, MNRAS, 413, 1828.

Zugger, M., Kasting, J.F., Williams, D.M., Kane, T.J., Philbrick, C.R., 2010, ApJ, 723, 1168.